

Artificial Skin for Humanoid Robots



Marco Maggiali
Italian Institute of Technology
University of Genova

A thesis submitted for the degree of
Philosophiæ Doctor (PhD), DPhil,..

November 2008

1. Reviewer:

2. Reviewer:

Day of the defense:

tee: Signature from head of PhD commit-

Contents

| | |
|--|-------------|
| List of Figures | v |
| List of Tables | xi |
| Glossary | xiii |
| 1 Introduction | 1 |
| 1.1 Introduction | 1 |
| 2 State of the Art | 3 |
| 2.1 Tactile and force sensors for robots and robot hands | 3 |
| 2.2 Tactile Sensors for Robot Hands | 4 |
| 2.3 Large Scale Tactile Sensors | 7 |
| 3 Tactile Sensor Design | 17 |
| 3.1 Tactile Sensor, a system level approach | 17 |
| 3.1.1 Transducers | 18 |
| 3.1.2 Measures | 19 |
| 3.1.3 Structure | 21 |
| 3.1.4 Architecture | 21 |
| 3.1.5 Data Processing | 22 |
| 3.1.6 Discussion | 23 |
| 4 Artificial Skin: Proposed Design | 25 |
| 4.1 Introduction | 25 |
| 4.2 Transducer | 25 |

CONTENTS

| | | |
|----------|---|-----------|
| 4.2.1 | Capacitive Sensor | 25 |
| 4.2.2 | Relaxation Oscillator Circuit | 26 |
| 4.2.3 | Materials | 29 |
| 4.3 | Measures | 30 |
| 4.4 | Structure | 30 |
| 4.5 | Architecture | 30 |
| 4.6 | Data Processing | 31 |
| 5 | Simulations | 35 |
| 5.1 | Introduction | 35 |
| 5.2 | Variable Capacitor Characterization | 35 |
| 5.2.1 | Capacitance VS Area | 38 |
| 5.2.2 | Capacitance VS Dielectric Constant | 38 |
| 5.2.3 | Capacitance VS Variable Relative Permittivity | 38 |
| 5.3 | Discussion | 38 |
| 6 | Design of a prototype | 43 |
| 6.1 | Introduction | 43 |
| 6.2 | Triangle Module | 43 |
| 6.3 | Microcontroller Board | 46 |
| 6.4 | Software for Data Acquisition | 48 |
| 6.5 | Hexagon prototype | 49 |
| 6.5.1 | Prototype on a 3D curved surface | 49 |
| 6.5.2 | Prototype on the iCub palm | 52 |
| 6.6 | Skin Graphical User Interface | 54 |
| 7 | Experiments | 59 |
| 7.1 | Introduction | 59 |
| 7.2 | Experimental Setup | 59 |
| 7.3 | Experiments on a triangle module | 61 |
| 7.3.1 | First Experiment: Sensor Response with a 12mm probe | 61 |
| 7.3.1.1 | Static Response | 61 |
| 7.3.1.2 | Low Frequency Response | 62 |

CONTENTS

| | | |
|-----------|--|------------|
| 7.3.2 | Second Experiment: Sensor Response with a 12mm probe reading macro-areas | 66 |
| 7.3.2.1 | Static Response | 66 |
| 7.3.2.2 | Low Frequency Response | 66 |
| 7.4 | Third Experiment: Sensor Response with a uniform pressure distribution | 66 |
| 7.5 | Fourth Experiment: Static and Dynamic Response for a triangle covered by 1mm of neoprene | 72 |
| 8 | Discussion | 79 |
| 8.1 | Problems and Future Works | 80 |
| 9 | Publications | 83 |
| 9.1 | Journal publications | 83 |
| 9.2 | Conference papers | 84 |
| 9.3 | Book Chapters | 85 |
| 10 | Patents | 87 |
| A | CANbus communication protocol | 89 |
| A.1 | Introduction | 89 |
| A.1.1 | Protocol Command Messages | 90 |
| B | Triangular Module Schematic and Layout | 93 |
| B.1 | Introduction | 93 |
| C | MCU Module Schematic and Layout | 97 |
| C.1 | Introduction | 97 |
| | References | 101 |

CONTENTS

List of Figures

| | | |
|------|---|----|
| 1.1 | The tactile sensor PCB rests on a human hand | 2 |
| 2.1 | DLR-II Hand.(Butterfass J. (2001)). | 5 |
| 2.2 | Embedded electronics of the DLR-II finger (Butterfass J. (2001)). | 6 |
| 2.3 | Gifu hand III and skin-like tactile sensors (H. Kawasaki and Uchiyama (2002);T. Mouri and Ito (2002)). | 6 |
| 2.4 | CyberHand | 8 |
| 2.5 | Robonaut Hand. | 8 |
| 2.6 | Placement of the pressure transducers in the Robonaut hand (T. B. Mar- tin and J.Butzer (2004)). | 9 |
| 2.7 | Detail of the Robonaut skin (T. B. Martin and J.Butzer (2004)). . | 9 |
| 2.8 | Tactile sensor sheet (Ohmura 2006). | 10 |
| 2.9 | Integration of the robot skin on the robot (Ohmura 2007) | 11 |
| 2.10 | Tactile sensors for the RI-MAN humanoid robot (Mukai, 2008).) | 13 |
| 2.11 | The Humanoid robot ARMAR-III (T. Asfour and R. (2006)). . . | 13 |
| 2.12 | The humanoid robot Robovie-IIS (Tajika T. and H. (2006)). . . . | 14 |
| 2.13 | Arrangement of tactile sensor in Robovie-IIS (Tajika T. and H. (2006)). | 14 |
| 2.14 | Humanoid robot CB2 (T. Minato and M. (2007)). | 15 |
| 2.15 | Tactile sensor layout of robot CB2 ((T. Minato and M. (2007))) . | 16 |
| 2.16 | Musculoskeletal humanoid Kotaro and the bandage tactile sensors (I. Mizuuchi and Inaba (2006)). | 16 |
| 3.1 | Tactile Sensor System schema. | 19 |
| 3.2 | Tactile Sensor Transducers. | 20 |

LIST OF FIGURES

| | | |
|-----|--|----|
| 3.3 | An example of a network for a large area tactile sensor system, (Y. Ohmura and Nagakubo (2006)). | 22 |
| 3.4 | The contact shape is modeled as an ellipsoid | 23 |
| 4.1 | Concept of the capacitive transducer. Typical model: finger varies circuit capacitance. | 26 |
| 4.2 | Concept of the capacitive transducer. A compliant ground plane changes the circuit capacitance when deformed by contact pressure | 27 |
| 4.3 | typical relaxation oscillator circuit topology is illustrated here . . | 28 |
| 4.4 | Frequency measurement involves measuring the relaxation oscillator frequency for a fixed time period using a gated time | 28 |
| 4.5 | Period measurement uses the oscillator frequency as a gate for a PWM | 29 |
| 4.6 | Example of a triangulation of a human hand using a computer graphic technique | 31 |
| 4.7 | System Architecture. Up to 16 tactile sensors (for a total of 192 taxels) can be networked and communicate with a microcontroller measuring pressure data and communicating with other modules using a CAN bus | 32 |
| 4.8 | System Architecture. Many mesh of triangles can be put side by side in order to cover a wider surface | 32 |
| 4.9 | CDC could read back each taxel for the maximum spatial resolution (a) or blocks of taxels augmenting the temporal resolution (b) | 34 |
| 5.1 | Characteristic of the CDC. It has been chosen a linear characteristic without considering the non linearity of the CDC (see AD7147 data sheet for more details) | 36 |
| 5.2 | Capacitance VS Distance curve for a capacitor with plates of 2mm radius | 37 |
| 5.3 | Capacitance and CDC output VS Area for a capacitor with plates from $10mm^2$ to $50mm^2$ | 39 |
| 5.4 | Capacitance and CDC output VS Distance curves for materials with dielectric constant from 1 to 7 | 40 |

LIST OF FIGURES

| | | |
|------|--|----|
| 5.5 | Capacitance VS Distance curve for materials either constant permittivity of 3 and variable permittivity from 1 to 7 | 41 |
| 6.1 | The triangle module. Each sensor implements 12 taxels and hosts the capacitive transduction electronics. | 44 |
| 6.2 | The thick layer of silicone rubber foam covering the sensors and the conductive layer used as ground plane sprayed on top. | 45 |
| 6.3 | 16 triangles interconnected on a flexible PCB | 45 |
| 6.4 | Microcontroller board. It is very compact in order to be installed inside the robot. | 47 |
| 6.5 | Library Blocks for the ESD-CAN usb to CAN converter in Simulink | 48 |
| 6.6 | Simulink Model for reading the triangles modules | 49 |
| 6.7 | The board is inserted on a PTFE mold with the electrodes side turned towards the bottom of the mold | 50 |
| 6.8 | After the placing of the board the mold is poured with silicone rubber foam | 50 |
| 6.9 | The board is turned 180 degrees | 51 |
| 6.10 | After the placing of the board the mold is poured with silicone rubber foam | 51 |
| 6.11 | A conductive layer is glued on the surface of the sensor | 52 |
| 6.12 | The hexagon has been installed on a 3D surface. The sensor can be curved to approximate the solid. | 53 |
| 6.13 | Multi-layer fiberglass mold and the carbon fiber palm of the robot (a). The mold fits the palm and can be placed and removed (b) . | 55 |
| 6.14 | From the triangle sheets, four triangles are cut in order to fit on the palm. | 56 |
| 6.15 | The triangles are glued on the fiberglass mold. | 56 |
| 6.16 | The sensor is mounted on the palm (a). It is covered by a 1mm thick neoprene and a conductive fabric acts as the ground plane(b) | 57 |
| 6.17 | SKINGUI is a software to visualize the skin output. A colormap is used to represent the pressure exert on each taxel | 58 |

LIST OF FIGURES

| | | |
|------|--|----|
| 7.1 | Test setup with a load cell that can measure static forces. The off-center load cell (3 kg AL series, from Laumas) and the micrometer (TESA Micromaster IP54) are shown | 60 |
| 7.2 | The strain gage amplifier used for the loadcell (Precise Instrument AT-10). | 60 |
| 7.3 | The circle represents the probe of the pressure. The central pads in blue are under the probe, the six in black are the one closed to the probe and the three in red in the angles are far from the probe. | 62 |
| 7.4 | A load/unload cycle, with a 12mm probe on the center of the triangle. As you can see there are three taxels with an higher response (the three under the probe), 6 with a small response (the neighbors) and 3 representing the angles of the triangle where the signal is stable. | 63 |
| 7.5 | Taxels versus Loadcell characteristic. | 63 |
| 7.6 | Taxels versus Deformation characteristic. As you can see the hysteresis here is much less then in figure 7.5, that means that part of the hysteresis is due to the loadcell as shown in figure 7.7. | 64 |
| 7.7 | The hysteresis of the load cell during a static load and unload cycle. It is clear how big it is with respect to the one of the sensor (figure 7.6). | 64 |
| 7.8 | Two load and unload cycles. | 65 |
| 7.9 | Taxels versus Loadcell characteristic. | 65 |
| 7.10 | Taxels versus Loadcell characteristic of three macro-areas. | 67 |
| 7.11 | Taxels versus Deformation characteristic of three macro-areas | 68 |
| 7.12 | Taxels versus Loadcell characteristic of one macro-area. | 69 |
| 7.13 | Taxels versus Deformation characteristic of one macro-area. | 69 |
| 7.14 | Load and Unload cycle reading three macro areas of the triangle | 70 |
| 7.15 | Taxels versus Loadcell characteristic reading three macro areas of the triangle | 70 |
| 7.16 | Load and Unload cycle reading one macro area of the triangle | 71 |
| 7.17 | Taxels versus Loadcell characteristic reading one macro area of the triangle | 71 |

LIST OF FIGURES

| | | |
|------|--|----|
| 7.18 | The circle represents the probe of the pressure, that in this case is bigger than the triangle. Therefore the pressure is uniform over the sensor. | 72 |
| 7.19 | Load and Unload cycles for a uniform pressure over the triangle module | 73 |
| 7.20 | Taxels versus Loadcell characteristic for a uniform pressure over the triangle module | 73 |
| 7.21 | Taxels versus Deformation characteristic for a uniform pressure over the triangle module | 74 |
| 7.22 | Load and Unload cycles reading three macro-areas for a uniform pressure over the triangle module | 74 |
| 7.23 | Taxels versus Loadcell characteristic reading three macro-areas for a uniform pressure over the triangle module | 75 |
| 7.24 | Load and Unload cycles reading one macro-area for a uniform pressure over the triangle module | 75 |
| 7.25 | Taxels versus Loadcell characteristic reading one macro-area for a uniform pressure over the triangle module | 76 |
| 7.26 | Load and Unload cycles for a 12mm probe positioned in the center of the triangle module | 76 |
| 7.27 | Taxels versus Loadcell curve for a 12mm probe positioned in the center of the triangle module | 77 |
| 7.28 | Taxels versus Deformation curve for a 12mm probe positioned in the center of the triangle module | 78 |
| B.1 | Schematic of the triangle module | 94 |
| B.2 | Layout of the triangle module, top (A), inner layer 1(B) and 2 (C) and bottom (D) | 95 |
| B.3 | Layout of the triangles sheet | 96 |
| C.1 | Schematic of the MCU board | 98 |
| C.2 | Layout of the MCU board, top (A) and bottom (B) | 99 |

LIST OF FIGURES

List of Tables

| | | |
|-----|--------------------------------|----|
| A.1 | Canbus Message frame | 90 |
| A.2 | Command Frame | 90 |

GLOSSARY

Glossary

| | |
|------------|---------------------------------|
| CDC | Capacitive to Digital Converter |
| MCU | Microcontroller Unit |
| TSM | Tactile Sensor Module |
| PCB | Printed Circuit Board |
| I2C | Inter Integrated Circuit |

GLOSSARY

Chapter 1

Introduction

1.1 Introduction

Tactile sensing is strategic for safe interaction of robots with humans, objects, and possibly in an unstructured environment. In fact, contact sensing provides the most important and direct feedback to control contact both in case of voluntary and non-voluntary interactions with the environment. Beyond the classical robot interaction tasks (e.g. *peg-in-hole* problem) where interaction is expected or planned at a specific robot location (typically at the end-effector tip), more advanced applications require more complex forms of interaction (e.g. whole hand or whole arm grasping and manipulation, gait stability control etc.), where the location and the characteristics of the contact could not be exhaustively predicted or possibly modeled in advance. In order to tackle these new issues sensor systems have to be developed to measure interaction phenomena over large contact areas. These sensor systems have to be properly interfaced to motor control modules to ensure reactive and safe interaction of the robot with the environment.

This thesis discusses the design of a large area tactile sensor to be integrated on a humanoid robot. The sensor should provide pressure and shape information about the contact of the robot with the environment. Ideally, the sensor would be a contained solution with embedded electronic that could be mounted on the robot external surface. This is a fundamental requirement, in fact, the purpose of this thesis is to design a tactile sensor that could be integrated on a robot, therefore the requirements are mainly the reduction of the number of wires and

1. INTRODUCTION

the size of the driving circuit. The system should be modular and scalable in order to be tailored to different parts of the robot's body, and should have a scalable sensitivity range in order to detect small pressures (i.e. in the arms) or very high pressures (in the feet). Furthermore because of the distributed sensors, the networking of the system has interesting aspects to be investigated: compression algorithms for reducing the bandwidth of the local bus, preprocessing techniques of the tactile data. In this thesis we have not explored this aspect, but we have designed the system in terms of hardware and networking in order to be able to implement such techniques in the future.

The state of the art is reported in chapter 2. Chapter 3 describes the requirements of tactile sensor for a humanoid robot application. We discuss her the approach adopted for the design of such a tactile sensor. The design of a novel artificial skin is presented in chapter 4. Simulations of the sensors are reported in chapter 5. The development of the prototype is discussed in chapter 6. Experimental data in chapter 7. Finally, discussion and future directions in chapter 8.



Figure 1.1: The tactile sensor PCB rests on a human hand

Chapter 2

State of the Art

2.1 Tactile and force sensors for robots and robot hands

Tactile sensing in robotics has been widely investigated in the past 30 years (Lee and Nicholls (1999)), and has received particular attention lately for the problem of grasping control with robot hands (H. Kawasaki and Uchiyama (2002), T. B. Martin and J. Butzer (2004), G. and M. (2005), B.B. Edin and M.C. Carrozza (2006), H. Liu and Hirzinger (1995)), but also for sensing contacts over robot links (T. Asfour and R. (2006), Tajika T. and H. (2006)) in order to enable safe interaction between humanoid robots and humans. Research in this field has focused largely on transduction principles and transduction technology: as a matter of fact a wide range of transduction solutions have been proposed (Lee and Nicholls (1999)). Most of the devices were either of the scalar *single-point* contact variety or were linear or rectangular arrays of sensing elements. The main transduction methods identified belong to the following classes: resistive, capacitive, piezoelectric and pyroelectric, magnetic, optical, ultrasonic. Despite the efforts made to prove the effectiveness of different type of transduction principles, various issues have strongly limited the development of embedded solutions for both robot hands and large area tactile sensors (robot skin in the following) and their actual application by the robotic scientific community. On one hand developing a tactile sensor is a very hard problem involving several engineering issues and often also

2. STATE OF THE ART

special processing equipment. Furthermore, there are at the bottom various technological difficulties which represent the bottleneck limiting the transition from a single tactile element (or a small matrix prototype) to a large scale integrated solution (e.g. the curse of wiring). This chapter is a short survey of various recent and interesting literature addressing the problem of designing sensorized robot hands as well as robot skin mostly at the system level. The objective is to provide a state of the art of tactile sensors from a system level point of view, emphasizing the issues of integration of the transducers with the electronic and mechanical hardware. Also, we will focus on standard transduction techniques (piezo-resistive, piezo-electric, capacitive and optical being the most common), since we assume that these principles are currently the best candidates for in-house custom development of embedded tactile sensing devices.

2.2 Tactile Sensors for Robot Hands

For manipulation and grasping, robots must be capable controlling the forces arising at the contact points. If the geometry of the gripper or robot hand is well known and the contacts can be modeled as point wise, it is possible to compute (or estimate) the contact location as well as the applied force using a six-axes force/torque intrinsic tactile sensor as discussed in (Bicchi. A and Brock (1993)). However, this minimalistic approach may fail when more complex interactions arise (e.g. in the case of multiple contacts, or contacts with non rigid objects etc.). In the latter case, the geometry of the contacts as well as pressure distributions must be measured directly using skin-like sensors. The design of distributed tactile sensors for robotic applications has been widely discussed in recent years (M. (2004); M. and K. (2002); Yamada K. and Shinoda (2002); Engel J. and Shannon (2003).). However, there has been an only limited number of papers discussing the integration and embedding of these devices on dexterous robotic hands. As a matter of fact, miniaturization and cabling harness still represent one of the most important limitations to the design of small sized embedded sensors. The four-fingered hand DLR-II (Butterfass J. (2001)), figure 2.1, is a significant example of robot gripper integrating a complete force/torque sensor system on

2.2 Tactile Sensors for Robot Hands

board . This hand has 22 degrees of freedom (DOFs) and is a complete self-contained system including motors, electronics and sensors. A sophisticated six-component force/torque transducer is installed on each fingertip and connected with the electronic modules, hosted on the palm of the hand, by ten wires (8 for data and 2 for power supply), figure 2.2. The DLR-II does not make use of tactile sensors and can detect contacts located only on its fingertips.

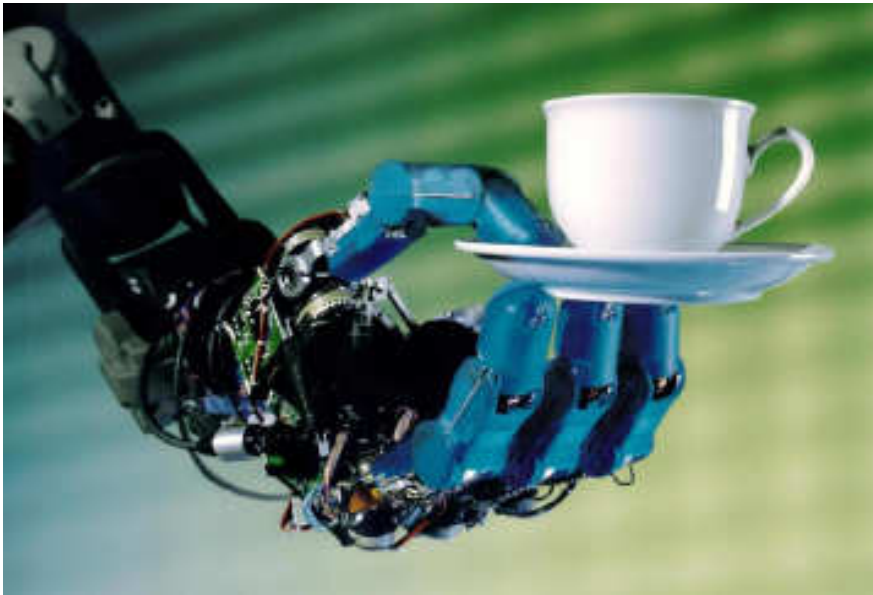


Figure 2.1: DLR-II Hand.(Butterfass J. (2001)).

The GIFU hands II and III (H. Kawasaki and Uchiyama (2002);T. Mouri and Ito (2002)), figure 2.3, have a commercial six axis force/torque sensor (produced by BL. AUTOTECH) integrated on each fingertip. However, these hands also feature a distributed tactile sensor based on pressure sensitive piezo-resistive ink transducers, see figure 2.3. The tactile sensor has 859 taxels formed by various grids of electrodes; the palm, the thumb, and each of the other fingers have 313, 126, and 105 taxels respectively covering about 50 % of the transducer's area. The sensor can withstand a maximum pressure load of about $2.2 \times 10^{-3} \text{ N} \div \text{m}^2$, with a resolution of 8 bits. The sampling cycle is 10 ms/Frame. The sensor is about 0.2 mm thick and can cover both planar and cylindrical surfaces. The hand does not embed the sensor electronics and sensor cables from the transducers and sensors are all routed along the fingers and palm.

2. STATE OF THE ART

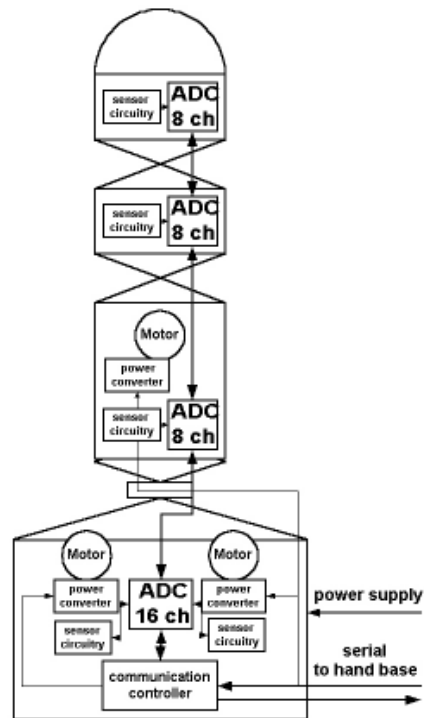


Figure 2.2: Embedded electronics of the DLR-II finger (Butterfass J. (2001)).

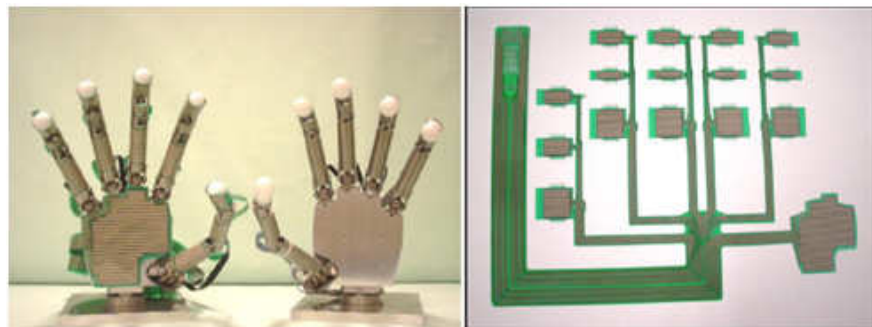


Figure 2.3: Gifu hand III and skin-like tactile sensors (H. Kawasaki and Uchiyama (2002); T. Mouri and Ito (2002)).

2.3 Large Scale Tactile Sensors

Another interesting example of integrated mechanical and sensing design is the robot hand CyberHand, a five fingered tendon driven under-actuated gripper, (B.B.Edin and M.C.Carrozza (2006)), figure 2.4. Each finger has on its tip a custom three axis force transducer, while the phalanges are sensorized with custom flexible polyimide sensor formed by on-off taxels, with an activation force of about 1N. Also in this case, the design of the sensors does not feature embedded electronics on the finger. This kind of skin sensor can provide only geometrical contact information, therefore cable-tension sensors based on strain gages have been integrated to estimate the force applied at the contact. In the Robonaut hand (T. B. Martin and J.Butzer (2004)), figure 2.5, a different approach to skin-like tactile sensing has been proposed. Instead of integrating the transducers on the mechanical structure of the hand, a sensorized glove covering the hand and embedding force transducers and cabling has been developed. The proposed design is based on a coarse grain distribution of pressure sensitive resistive rubber transducers (produced by QTC Ltd. and Interlink Inc.), figure 2.7. In total the glove has 33 sensitive sites where contact forces are concentrated by means of plastic beads, 2.6. The concept is simple and the adoption of discrete piezo-resistive resistive transducers suggests that this solution could be used for simple custom tactile sensors, also because interface electronics consists only of a voltage divider. There are however some drawbacks quoted by the authors. In fact, as the hand opens and closes the glove itself applies forces on the transducers; furthermore the glove interfere with the hand movements. Both problems have been addressed in (T. B. Martin and J.Butzer (2004)), but the authors considered them still open issues.

2.3 Large Scale Tactile Sensors

From the previous section it emerges that a major issue for designing tactile sensors for grasping and manipulation is related to the need of tailor-made solutions. In fact, most of the solutions proposed are strongly dependent on the mechanical design and specialized for a particular platform. Other features like modularity and scalability could in fact improve the characteristics of these devices. The target is that of developing modular sensors, with embedded transducers and

2. STATE OF THE ART

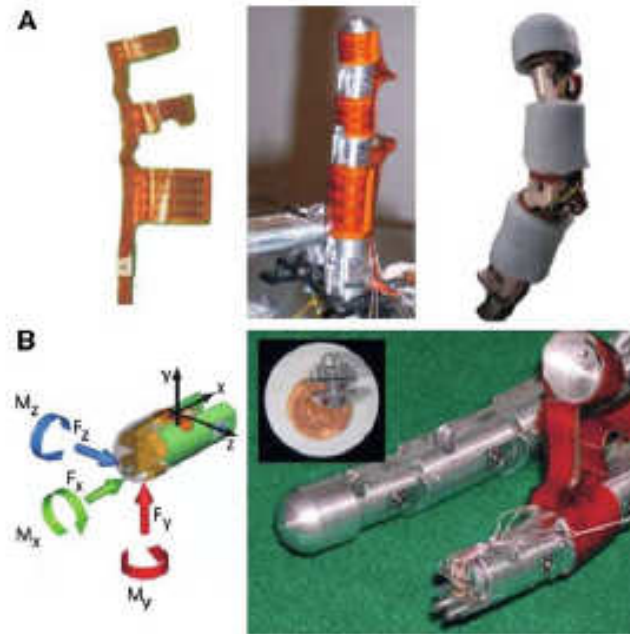


Figure 2.4: Cyberhand tactile sensor.



Figure 2.5: Robonaut Hand.

2.3 Large Scale Tactile Sensors



Figure 2.6: Placement of the pressure transducers in the Robonaut hand (T. B. Martin and J. Butzer (2004)).

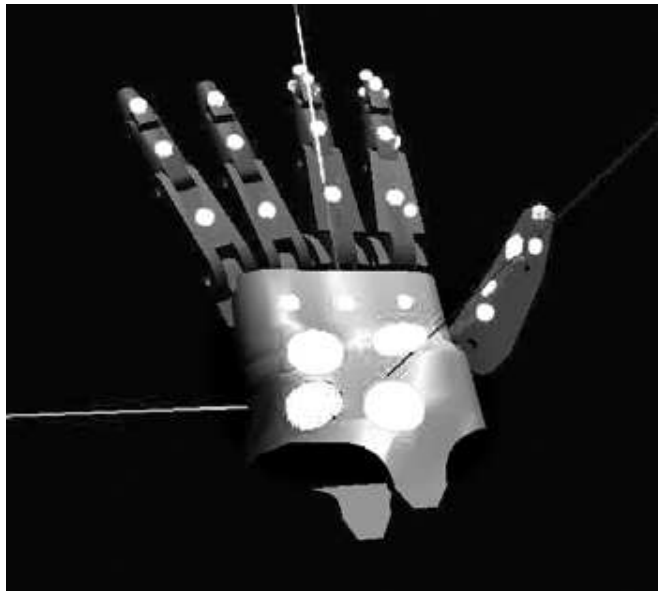


Figure 2.7: Detail of the Robonaut skin (T. B. Martin and J. Butzer (2004)).

2. STATE OF THE ART

electronics possibly based on a common design. Networking of these devices would enable scalability and incremental development of large scale tactile sensors. These ideas have been used for the design of various large scale skin-like sensors proposed in the literature. By large scale we intend tactile sensors which can cover large areas of a robot body conforming to its outer shape. The investigation on large scale robot skin has originally received attention for particular applications, as space robotics (Lumelsky V.J. and S. (2001)), but it significantly increased recently with the growth of the interest in humanoid robots. A humanoid robot is expected to interact in complex and largely unpredictable way with the environment, and it is expected to be capable of safe and purposive interaction with humans (A.Billard and Siegwart (2004)). The class of humanoid robot tasks requiring direct interaction capabilities is certainly much larger and critical than those addressed in the past. Complex operations involving concurrent walking, interaction with humans and body manipulation (Y. Ohmura (2007)) are strongly based on active control relying also on tactile feedback. In fact, these tasks need the monitoring of the contacts of the robot with the environment which may happen at unpredictable positions and in unpredictable ways.

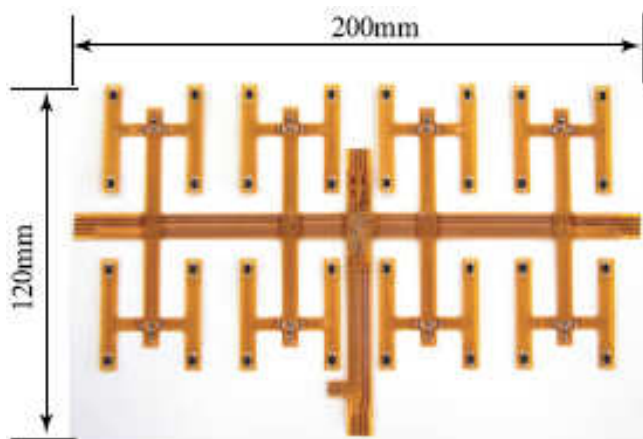


Figure 2.8: Tactile sensor sheet (Y. Ohmura and Nagakubo (2006)).

One of the first examples of truly scalable robot skin systems for humanoid robots has been proposed by Ohmura and Kuniyoshi (Y. Ohmura and Nagakubo

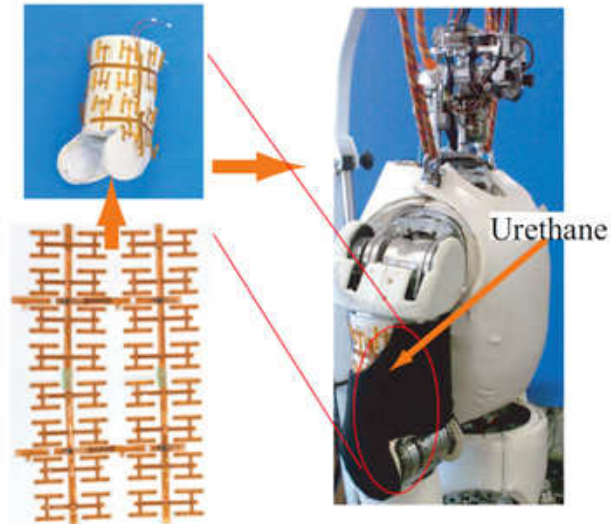


Figure 2.9: Integration of the robot skin on the robot (Y. Ohmura and Nagakubo (2006)).

(2006)). They approached the problem at system level, and focused on the issue of the wiring as the key problem for developing a technology amenable to practical implementation. Their main contribution has been that of introducing a networked architecture featuring peripheral nodes (chips) scanning (locally) a limited number of taxels. The electronics and the transducers are embedded on a tree-shaped flex/semi-flex PCB support, figure 2.8. This solution allows a simple mechanical integration of the sensor over curved surfaces and has been experimentally tested with success (Y. Ohmura (2007)), figure 2.9. This system design has however some limitations. The spatial resolution is quite low since the minimum distance between the taxels is about 2.7 cm. Furthermore, the sensor is based on IR optical transducers which have (at the present status of the technology) a quite large power consumption; this means that for a complete robot skin system (which might have thousands of taxels) the power supply requirements becomes critical (e.g. for autonomous robots). An attempt to limit the power consumption works by sequencing the switching of the LEDs and this clearly reduces the sampling rate capability of the sensor. Finally, other limitations of this design are related to the network solution adopted which does not seem to support fault

2. STATE OF THE ART

tolerant mechanisms. This is important because by its own nature the robot-skin is subjected to continuous or cyclic stress and impacts over long periods of time and its performance has to have graceful degradation. The fault tolerance problem was previously addressed by Um and Lumelsky (D. and Lumelsky (1999)), who worked via component redundancy for a system featuring over 1000 sensing elements.

A similar layout, but using piezo-resistive commercial pressure transducers has been recently proposed in (Mukai T. and Z. (2008)), figure 2.10. The sensor is modular, and consists of 8×8 taxels with a spatial resolution of 1.8 mm which can withstand a pressure of about 12 N/cm^2 . It does not embed electronics, however custom hardware modules for data acquisition and networking allow a scalable configuration of the system. The RI-MAN humanoid robot (Mukai T. and Z. (2008)), is equipped with five tactile modules for a total of 340 taxels and implements a tactile based feedback control operating at 50 Hz. In the robot ARMAR-III (T. Asfour and R. (2006)), figure 2.11, developed by Prof. Dillmann and his team, the idea of skin patches, based on piezo-resistive matrices of sensors, with embedded data processing electronics has been successfully implemented. Embedded electronics provides local tactile data processing in order to limit the bandwidth requirements. The patches are custom designed and have flat or cylindrical shape in 3D for covering relevant parts of the robot arms, while smaller patches are used to sensorize the fingers. Another example of artificial skin system for a humanoid robot has been proposed by Tajika et al. (Tajika T. and H. (2006)) and implemented in the Robovie-IIS, figure 2.12. The tactile sensors have been designed with the aim of detecting stimuli coming from people trying to interact with the robot and it is based on PVDF based transducers. The skin has low spatial resolution (transducer area is of about 25 cm^2). It can measure only stimuli at frequencies higher than 5-10 Hz, figure 2.13.

A similar solution has been adopted in the CB2 humanoid robot (T. Minato and M. (2007)). The robot it has human-like appearance similar to a child-size boy. It is about 130cm high and weights about 33kg, see figure 2.14. Tactile sensing is obtained by embedding small thin PVDF films beneath the skin. The system is not modular, i.e. the transducers are placed ad-hoc over the robot body. The output is proportional to the rate of change of bending (*deformation rate*).

2.3 Large Scale Tactile Sensors

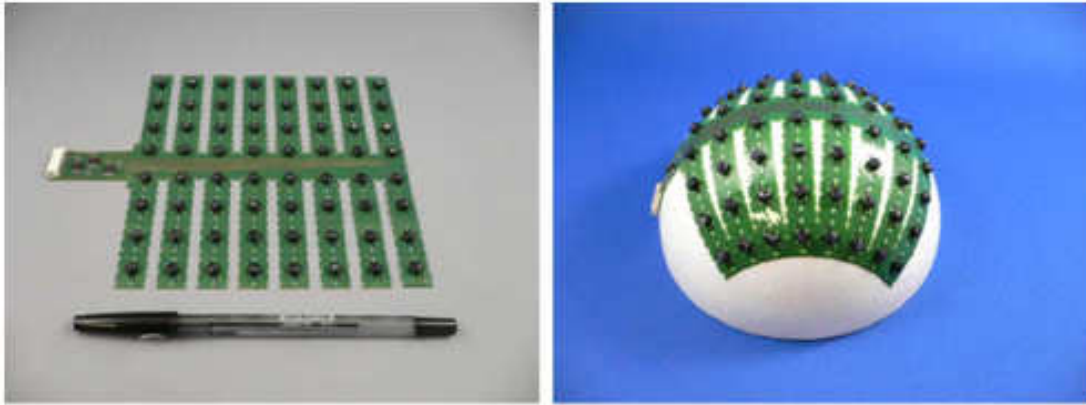


Figure 2.10: Tactile sensors for the RI-MAN humanoid robot (Mukai T. and Z. (2008)).



Figure 2.11: The Humanoid robot ARMAR-III (T. Asfour and R. (2006)).

2. STATE OF THE ART



Figure 2.12: The humanoid robot Robovie-IIS (Tajika T. and H. (2006)).

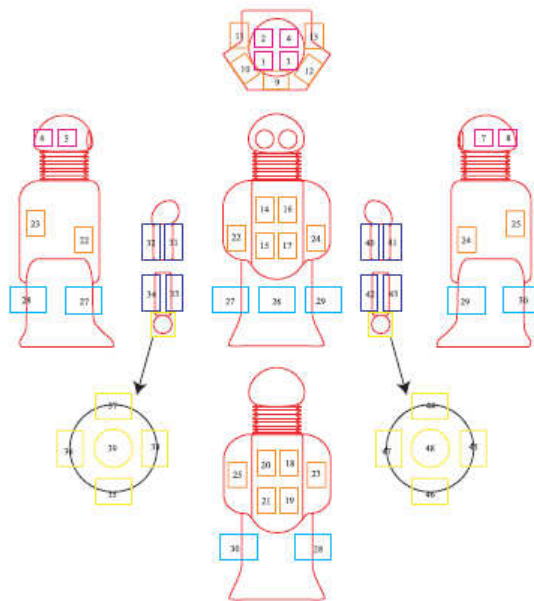


Figure 2.13: Arrangement of tactile sensor in Robovie-IIS (Tajika T. and H. (2006)).

2.3 Large Scale Tactile Sensors

The information equivalent to a contact force is obtained by temporal integration of the sensor output. The transducers are put between a layer of urethane foam covering the mechanical parts and the outer silicone skin. On the robot there are 197 sensors providing output at a frequency of 100 Hz, figure 2.15.



Figure 2.14: Humanoid robot CB2 (T. Minato and M. (2007)).

Finally, Kotaro (I. Mizuuchi and Inaba (2006)), is a very complex musculo-skeletal humanoid robot where tactile sensing is obtained using flexible bandages formed by two flexible printed circuit boards with a intermediate layer of pressure-sensitive conductive rubber forming 64 taxels. The sensor can match complex shape surfaces, figure 2.16.

2. STATE OF THE ART

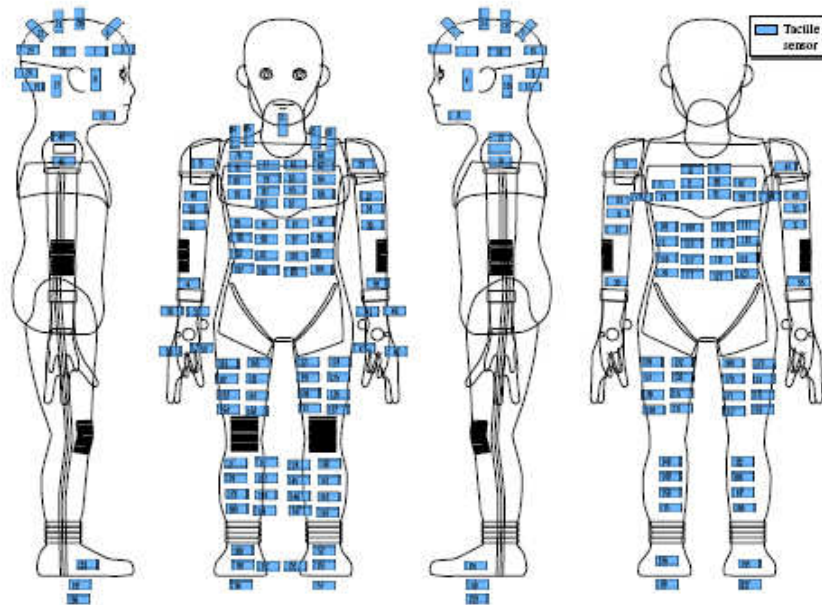


Figure 2.15: Tactile sensor layout of robot CB2 ((T. Minato and M. (2007)))

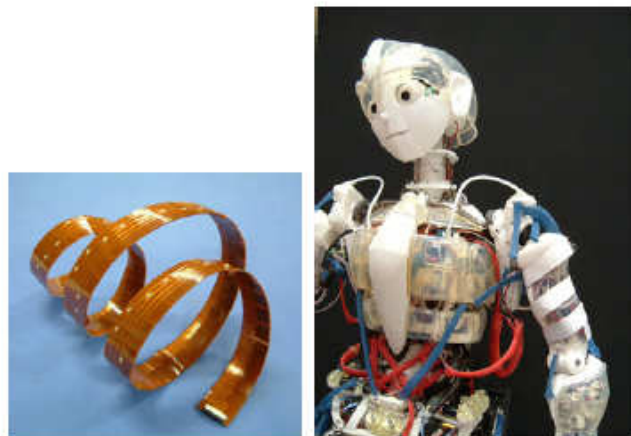


Figure 2.16: Musculoskeletal humanoid Kotaro and the bandage tactile sensors (I. Mizuuchi and Inaba (2006)).

Chapter 3

Tactile Sensor Design

3.1 Tactile Sensor, a system level approach

We think that a system level approach is needed for the design of an artificial skin for robotic applications. This is because moving from the single tactile element to thousands of sensors covering the whole body of a robot is not straightforward. There are many problems to solve: cabling, dimensions, data processing and data communication, manufacturing, etc. Therefore it is important to evaluate all the parts forming the whole system from the beginning. The criteria used during the decision process are not very well defined in the literature. There is not a *receipt book* for making an artificial skin. There are some features and very general guidelines (Y. Ohmura and Nagakubo (2006)) that are summarized in the following list:

- *conformability*: the skin should be applicable to arbitrarily curved surfaces (without specifically fabricating different sensor units for each curved part which is overwhelmingly expensive).
- *compliance*: the sensor should have a soft surface (some tactile sensors are rigid and not appropriate for whole-body contact motions);
- **Dynamic range and sensitivity**: The sensors should be able to detect contact between light touch and total bodyweight.

3. TACTILE SENSOR DESIGN

- Installation space: should be kept to a minimum because the interior of the robots shell is full of mechanisms and circuits.
- Area coverage: should be as large as possible (keeping the wiring to a minimum and taking into account difficulty of implementation).
- Weight: the skin should be light-weight because it has potentially to cover the entire body surface which is a large area (i.e. sensor weight can be a big problem).
- *power consumption*: the power consumed by the individual tactile elements should be low (an increase of the number of sensors makes it large).
- *size*: the individual sensing elements should be of small size (higher sensing resolution).
- *toughness*: the skin should be tough and robust against impact and shear forces.
- *manufacturing*: the skin should be easy to manufacture (in particular for low volume production)

During the design we have considered these aspects and we discuss them further in next chapters.

From a system level point of view , in order to undertake the design of an artificial skin system, we divide the system in five main parts as sketched in figure 3.1 and detailed in the following.

3.1.1 Transducers

Conventional tactile sensors have been exploited from various physical transduction principles. They record the phenomena of the contact because of the transduction of certain physical quantities (e.g. pressure) into other (e.g. change displacement) that are measurable as electrical signals. Strain gage, piezoelectric sensor, pressure sensitive rubber, photometric and pressure gage have been used (Lee and Nicholls (1999)). Figure 3.2 summarizes the main characteristics with pros and cons of the principal transducers used for tactile sensing.

3.1 Tactile Sensor, a system level approach

| | | |
|------------------------|--|--|
| Transducers | Which are the technologies to get the contact? | <ul style="list-style-type: none"> • Conductive Rubber • Conductive and Resistive Ink • Silicone • Anisotropic transducer • ... |
| Measures | Which contact characteristic is acquired? | <ul style="list-style-type: none"> • Static • Dynamic |
| Structure | The geometry of the sensible elements | <ul style="list-style-type: none"> • Taxel-like forms • Molded cover |
| Architecture | HW/SW for acquisition and signal conditioning | <ul style="list-style-type: none"> • signal conditioning • Microcontroller units • External Communication • Local Communication |
| Data Processing | Processing for the control (but not only) | <ul style="list-style-type: none"> • Data compression • "Smart" algorithms to reduce the sending of useless data. |

Figure 3.1: Tactile Sensor System schema.

3.1.2 Measures

The contact between two object can be divided in three main phases: the collision, a static contact and/or a shear. During collision, the force of the deformation will absorb most, or even all, of the force of the contact. Viewed from the conservation of energy perspective, the kinetic energy of the objects is changed into heat and sound energy, as a result of the deformations and vibrations. To measure force vibrations and temperature applied during a collision, high frequency measurements are required (100Hz-10KHz). For static contact we intend the phase that may occur after the collision if the objects remain in contact without shear. In this case low frequency measurements well describe the contact (1Hz-100Hz). Shear, may occur if the contact is not stable and there is a sliding between the two objects. It generates vibrations and therefore even in this case high frequency measurements must be done (100Hz-10KHz). Therefore, there are many measurements that can be done in order to describe contact. The classification regards the frequency domain of the measurements: static (from 0 to 100 hertz) and dynamic, (from 100 Hz and above). With the current technologies, we can measure at low speed (1Hz-100Hz) contact pressure distribution, contact shape, temperature data, deformation rate. With dynamic measurements (100Hz-10KHz) it is possible to get strain and shear stress, and vibrations. A robot should have sensors of both types in order to guarantee fast response to external stimuli (dy-

3. TACTILE SENSOR DESIGN

| Sensor Type | Sensor Attributes | Advantages | Disadvantages |
|--|--|---|---|
| <p>Piezoresistive Polymer Array</p> <p>Micromachined piezoresistive junctions made on silicon embedded on an elastomeric material, in order to increase the overload capability of the sensor</p> | <ul style="list-style-type: none"> • Array of piezoresistive junctions commonly embedded in a elastomeric skin • most commonly cast or screen printed | <ul style="list-style-type: none"> • Simple design • Simple signal conditioning | <ul style="list-style-type: none"> • Often fail -> short life • Subject to signal drift and hysteresis |
| <p>TouchScreen like</p> <p>They use the same structure of a touchscreen, adding in same case the possibility to measure also the force applied in the touchscreen surface</p> | <ul style="list-style-type: none"> • Large area taxels | <ul style="list-style-type: none"> • Low force thresholds / high sensitivity • Simple design • Simple signal conditioning • Aggregate measure of pressure • reduction of wires | <ul style="list-style-type: none"> • Subject to signal drift and hysteresis |
| <p>Capacitive Array</p> <p>A capacitive touch sensor relies on the applied force either changing the distance between the plates or the effective surface area of the capacitor. In such a sensor the two conductive plates of the sensor are separated by a dielectric medium, which is also used as the elastomer to give the sensor its force-to-capacitance characteristics</p> | <ul style="list-style-type: none"> • Array of capacitive junctions • most commonly constructed of row and column electrodes separated by an elastomeric dielectric layer | <ul style="list-style-type: none"> • good sensitivity • moderate hysteresis, depending on mechanical construction | <ul style="list-style-type: none"> • complex circuitry. • stray capacitance |
| <p>Optical</p> <p>For robotic touch and force-sensing applications, the extrinsic sensor based on intensity measurement is the most widely used due to its simplicity of construction and the subsequent information processing. Extrinsic: where the physical stimulus interacts with the light external to the primary light path.</p> | <ul style="list-style-type: none"> • Based on tracking an array of dots inscribed on skin membrane | <ul style="list-style-type: none"> • uniformly thin, compliant membrane • no electrical interconnects to be damaged | <ul style="list-style-type: none"> • Complex computations required |
| <p>Magnetic</p> <p>The movement of a small magnet by an applied force will cause the flux density at the point of measurement to change. The flux measurement can be made by either a Hall effect or a magnetoresistive device</p> | <ul style="list-style-type: none"> • employs an array of hall effect sensors | <ul style="list-style-type: none"> • high sensitivity • high dynamic range • linear response | <ul style="list-style-type: none"> • Dimension • creep effect due to the elastomer |
| <p>PVDF</p> <p>Polymeric materials that exhibit piezoelectric properties are suitable for use as a touch or tactile sensors, while quartz and some ceramics have piezoelectric properties. polymers such as polyvinylidene fluoride (PVDF) are normally used in sensors.</p> | | <ul style="list-style-type: none"> • Dynamic response | <ul style="list-style-type: none"> • no continuous response |

Figure 3.2: Tactile Sensor Transducers.

3.1 Tactile Sensor, a system level approach

dynamic sensor) but also the capability to extract detailed information about the shape of the contact or the temperature value of the object that is in contact with the robot (static measurements). However multi-modal tactile sensor require different transduction technologies, different data processing and the complexity of the whole system leading to higher system complexity increases.

3.1.3 Structure

The structure represents the organization of the tactile sensor elements (taxels). In other words this refers to the approach adopted to integrate single sensor elements in a large scale skin. The structure defines the geometry of the sensing elements. Possible solutions are to design interconnected patch of taxels (Y. Ohmura and Nagakubo (2006)) or to tailor a custom geometry for every part of the robot, (T. Asfour and R. (2006), T. Minato and M. (2007)). There are pro and cons in both cases and in both cases there are mechanical and electronics problems to solve, that usually are specific of the particular sensor developed: transducer technology, signal conditioning, dimensions of the single element. In order to have a scalable and modular system the first solution is more indicated, but it is not always the best one in terms of wiring and spacing.

3.1.4 Architecture

The architecture of the system consists of hardware and software for acquisition and signal conditioning. Moreover, the system could include microcontrollers and network links. For example, the skin could have a local network between the microcontroller boards distributed on the robot and an external one from the MCU boards towards the central pc. It is important to define the architecture of the heterogeneous network in order to determine the bandwidth and the computational units needed and therefore the wiring and placing complexity. Figure 3.3 shows an example of network architecture implemented on a humanoid robot (Y. Ohmura and Nagakubo (2006)).

3. TACTILE SENSOR DESIGN

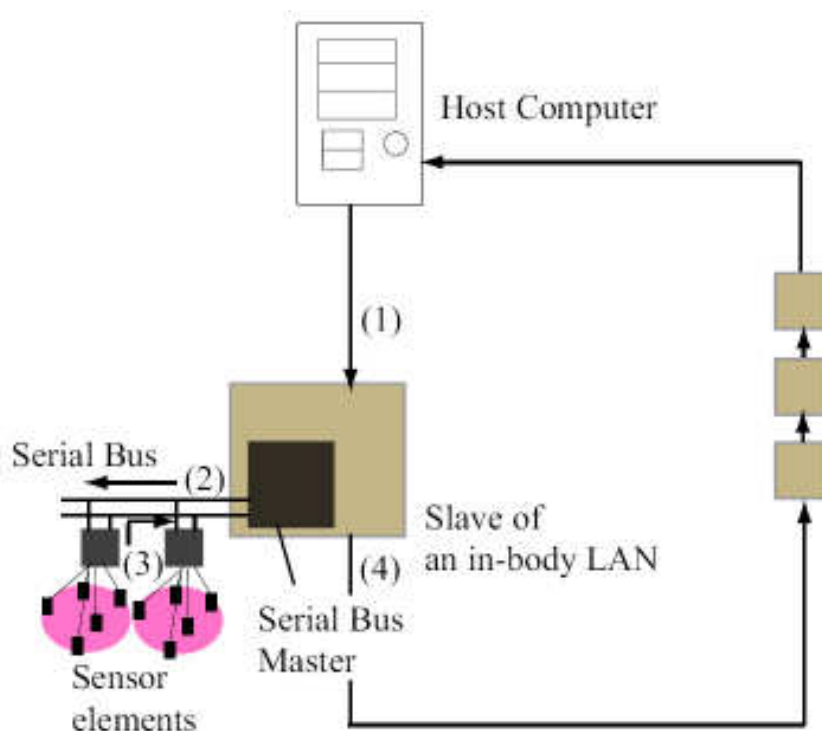


Figure 3.3: An example of a network for a large area tactile sensor system, (Y. Ohmura and Nagakubo (2006)).

3.1.5 Data Processing

Data processing is very important in case of an artificial skin because of the huge amount of data distributed on a wide surface. It means that a Therefore, it is important to define the strategy for processing data in local nodes and then send them to a central PC afterward. Compression algorithms usually adopted for compressing images can be used also for tactile images, but there are also more specific techniques that can be implemented. As example the *contact centroid estimation* (G. and M. (2006)) can be used, in order to reduce the amount of data characterizing the sensor. Let us assume that the contact between the sensor and an object, corresponds to a pressure distribution over a connected region. The distribution, in general, can not be assumed to be unknown a-priori and therefore is modeled as a random one. It is reasonable to associate the contact distribution (i.e. the tactile image), to statistical moments of the first and second order. In

3.1 Tactile Sensor, a system level approach

particular, it is possible to define the *pressure centroid* \mathbf{x}_c as follows:

$$\mathbf{x}_c = \frac{\sum_{i=1}^N \mathbf{x}_i p(\mathbf{x}_i)}{\sum_{i=1}^N p(\mathbf{x}_i)} \quad (3.1)$$

where \mathbf{x}_i are the position of each taxel in local surface coordinates, $p(\mathbf{x}_i)$ are the corresponding measured pressure and N is the number of taxels of the sensor. The *shape* of the pressure distribution could be approximated as an ellipsoid, (figure 3.4) , defined as follows:

$$E = \frac{\sum_{i=1}^N (\mathbf{x}_i - \mathbf{x}_c)(\mathbf{x}_i - \mathbf{x}_c)^T p(\mathbf{x}_i)}{\sum_{i=1}^N p(\mathbf{x}_i)} \quad (3.2)$$

where E is a positive semi-definite symmetric matrix.

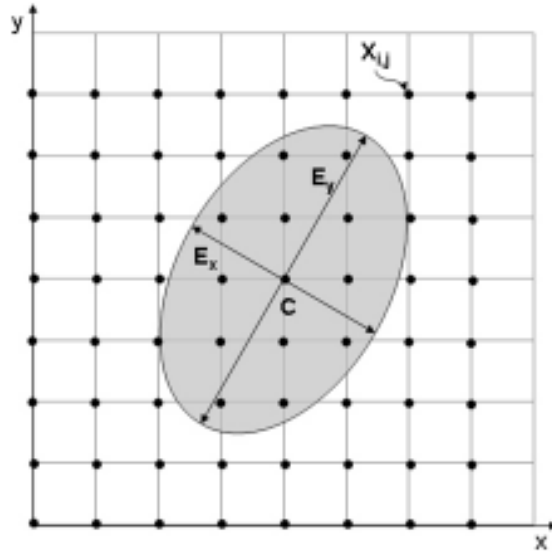


Figure 3.4: The contact shape is modeled as an ellipsoid

3.1.6 Discussion

We have seen that the artificial skin is a complex system and that for all the parts composing it, there are many possible solutions and drawbacks. There

3. TACTILE SENSOR DESIGN

is the choice of what we want to measure, the transducers, the electronics, the structure and the architecture of the system and also where to do the processing of the data. In the next chapter we provide a design of such a system, showing how we have find a feasible solution.

Chapter 4

Artificial Skin: Proposed Design

4.1 Introduction

This chapter describes the large area tactile sensor solution proposed. As shown in figure 3.1, an artificial skin system includes various elements to be considered, such as: the transducer, the types of measurements of interest, the structure of the system (taxels-like, molded), the hardware and the software architecture, and the data processing strategy. In the next sections we discuss the parts mentioned above, explaining the rationale of our choice. In section 4.2 the transducer technology we have used is described.

4.2 Transducer

After the analysis of the possible technological solutions (figure 3.2), the capacitive sensor technology has been selected as the best candidate for our purpose. It has good sensitivity, it has a simple structure and a good temporal response.

4.2.1 Capacitive Sensor

A capacitive tactile sensor is based on a capacitor, where the dielectric is made of a compliant material so that the capacitance changes due to the strain exerted on the sensor. In the proposed design, capacitive pressure transducers have been implemented using commercially available capacitance to digital converter

4. ARTIFICIAL SKIN: PROPOSED DESIGN

integrated circuits (CDC), commonly used for example in cell phones. The CDC detects the variation of a capacitance (4.2.2), e.g. due to the presence of a human finger over a copper plate: the closer the finger, the higher the variation. In our design the structure of the capacitor has been modified in order to recognize not only human touch but also non conductive objects. As shown in 4.1, a deformable conductive ground plane is introduced and the effect of contact pressure is a change of circuit capacitance. The ground plane, as show in 4.2, is implemented by spraying a thin layer of electrically conductive silicon rubber (connected to ground), over a thick (3-5 mm) compliant substrate made of silicone rubber foam, 3-5 mm). In this way, when any object is pressing the silicone rubber, in fact, the ground plane deformation, changes the capacitance value of the circuit. The ground plane forming the outer layer of the sensor has also the benefit of reducing the electrical noise coming from the environment.

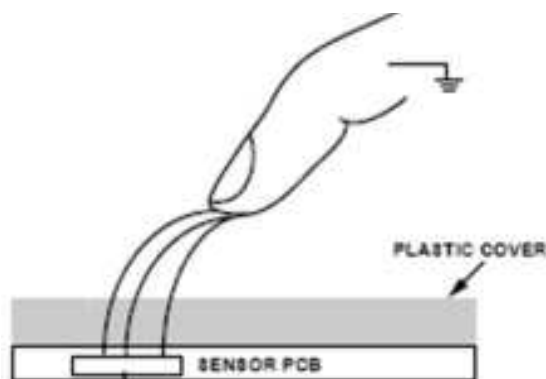


Figure 4.1: Concept of the capacitive transducer. Typical model: finger varies circuit capacitance.

4.2.2 Relaxation Oscillator Circuit

A relaxation oscillator is an effective and simple circuit for measuring capacitance (figure 4.3). This circuit consists of four components: a synchronous comparator, current source, discharge switch, and the capacitive sensor. Initially, the discharge switch is open, and the current source linearly charges the sensor. The voltage on the sensor ramps positively until it exceeds the comparator's threshold. The comparator's output transitions from low to high, causing the discharge switch to

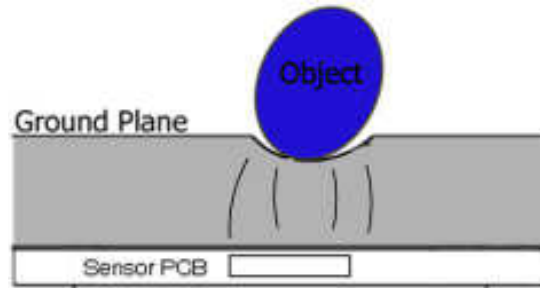


Figure 4.2: Concept of the capacitive transducer. A compliant ground plane changes the circuit capacitance when deformed by contact pressure

close. The sensor quickly discharges through this low impedance path to ground. The process causes the comparator's output to transition from high to low, and the cycle repeats. The output frequency (f_{out}) is dependent on the charging current and capacitive sensor value as illustrated by:

$$f_{out} = \frac{i_{charge}}{C_P V_{BG}} \quad (4.1)$$

Typical designs set the oscillator's frequency between 20 and 250 kHz. The frequency is then fed into an intelligent measurement circuit. By measuring the change in the frequency, it's possible to determine the capacitance change. There are two widely accepted methods for measuring the frequency of the relaxation oscillator. One method measures the frequency itself; the other method measures period.

Frequency measurement involves measuring the relaxation oscillator frequency for a fixed time period using a gated timer (figure 4.4). The timer is read to determine the number of counts accumulated during the fixed period. This method works well for slow frequencies where the discharge time of the capacitive sensor is negligible compared to the oscillator period.

Period measurement uses the oscillator frequency as a gate for a pulse-width modulator (PWM). The timer is clocked by a faster frequency than that of the relaxation oscillator (figure 4.5). The faster the timer clock, the better the resolution of the measured capacitance. Either method can be easily implemented

4. ARTIFICIAL SKIN: PROPOSED DESIGN

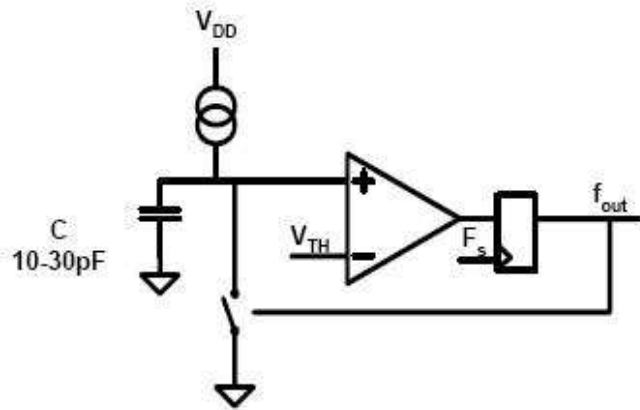


Figure 4.3: typical relaxation oscillator circuit topology is illustrated here

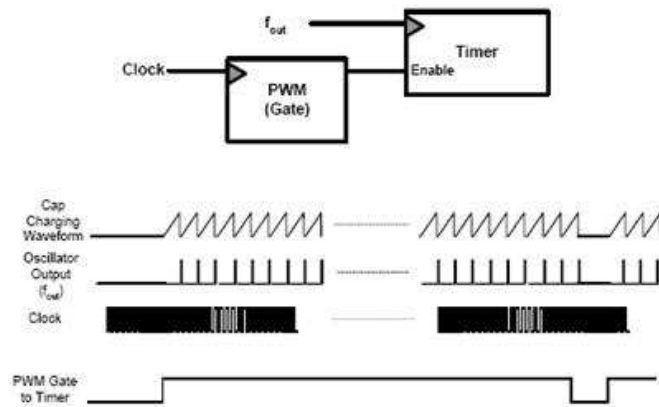


Figure 4.4: Frequency measurement involves measuring the relaxation oscillator frequency for a fixed time period using a gated time

with traditional 555 timers or more complex microcontrollers. Because an intelligent software algorithm is needed, a microcontroller-based solution seems more elegant.

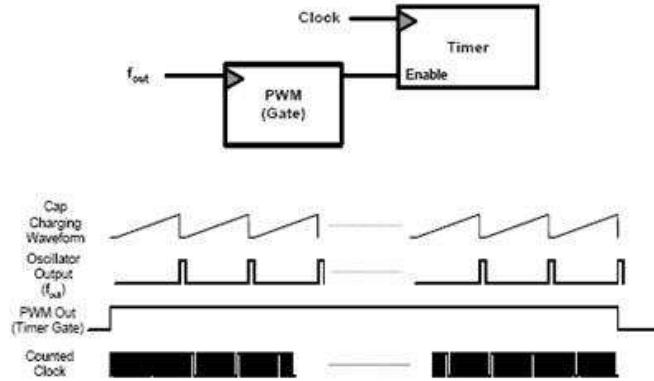


Figure 4.5: Period measurement uses the oscillator frequency as a gate for a PWM

4.2.3 Materials

One of the fundamental parts of the transducer is the soft layer that acts as the dielectric material in between the two plates. Indeed, variations of the capacitance are due to the variation of the dielectric thickness and permittivity. The formula relating capacitance with the physics of the capacitor is the following:

$$C = \varepsilon\varepsilon_0 \cdot \frac{A}{x} \quad (4.2)$$

where ε_0 is the permittivity of free space and ε the dielectric constant of the material used. A is the area of the plate and x is the distance between the two plates. Materials that are typically used are urethane foams, neoprene and silicone rubber foam. The softer the material lesser pressure is required for reducing the distance between the plates. However, if the material were too soft, then it would reach its minimum thickness too quickly. It is important to consider the dielectric properties of a material: the higher the relative permittivity the higher the sensitivity. Also in this case there is a drawback: increasing the relative permittivity of a silicon rubber for example using barium titanate or titanium

4. ARTIFICIAL SKIN: PROPOSED DESIGN

dioxide, increases the Young's modulus of capacitive sensors (it becomes stiffer). There is not a specific study about the materials. In chapter 5 we try to address the question via simulations including the relation between, the area of the plates, the dielectric constant and the distance. In chapter 7 there are examples of responses with different materials.

4.3 Measures

The sampling rate of capacitive technology is from one to a few hundreds Hz depending on the structure of the system and the architecture. Therefore we can get static and low frequency dynamic pressure measures. There are other aspects related to the particular structure we have used, that we will discuss later and are related to the possibility of changing the spatial versus temporal resolution ratio in order to increase spatial resolution for static or quasi-static measurements while the higher temporal resolution, at the price of spatial resolution, could be used for obtaining dynamic response.

4.4 Structure

The structure developed is new and it takes inspiration from computer graphics (figure 4.6). The idea was to use triangular modules, in order to approximate arbitrary surfaces, like computer graphics with triangularization techniques does. In this way we can cover with the skin mechanical parts with complex surfaces and the smaller the triangles the better the approximation. However, the difference with respect to computer graphics is that the triangles in our case are flexible, therefore, they can be better adapt on the surface. The first prototype we have build has triangles with the same size, but in the future we would have triangles with different size and shape.

4.5 Architecture

The architecture of the system consists of the signal conditioning electronics, computational units, cabling and networking. As mentioned above, the structure

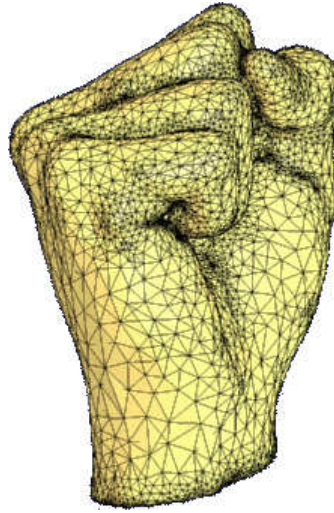


Figure 4.6: Example of a triangulation of a human hand using a computer graphic technique

of the system is based on triangular modules . Each module contains the signal conditioning electronics and 3 I/O ports, one input and two output ports. Therefore, it is possible to interconnect many triangles together forming a mesh (16 in the current solution for each MCU board), without wires, because the connections are etched on the flexible circuit. The mesh is connected through one cable to a microcontroller board (MCU board) that reads back the measurements from the triangles and can also provide computational power for data processing. Furthermore, the MCU board has a CANbus link in order to connect many boards together with a Supervisor PC (in the case of the humanoid robot iCub, a pc104 CPU installed in the head has a PCI-CAN interface). Figure 4.7 and 4.8 show the architecture of the entire system.

4.6 Data Processing

The proposed architecture provides local computation nodes distributed over the robot body. Moreover the single triangle has itself the possibility to change its behavior programmatically. Therefore in the current implementation, there are two levels of data processing (figure 4.8). The first one is in each triangular module, in fact, it is possible to program the CDC converter in order to modify

4. ARTIFICIAL SKIN: PROPOSED DESIGN

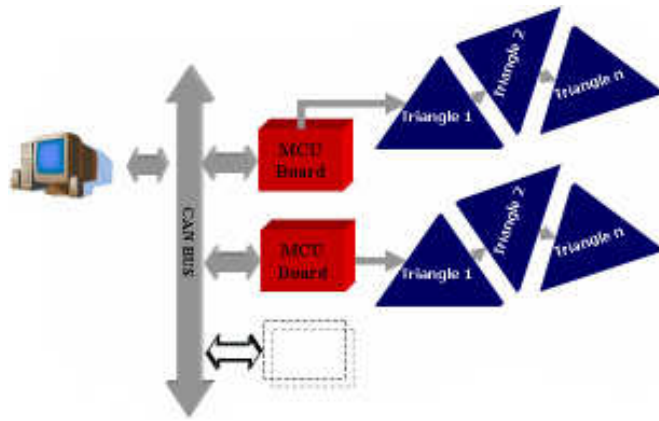


Figure 4.7: System Architecture. Up to 16 tactile sensors (for a total of 192 taxels) can be networked and communicate with a microcontroller measuring pressure data and communicating with other modules using a CAN bus

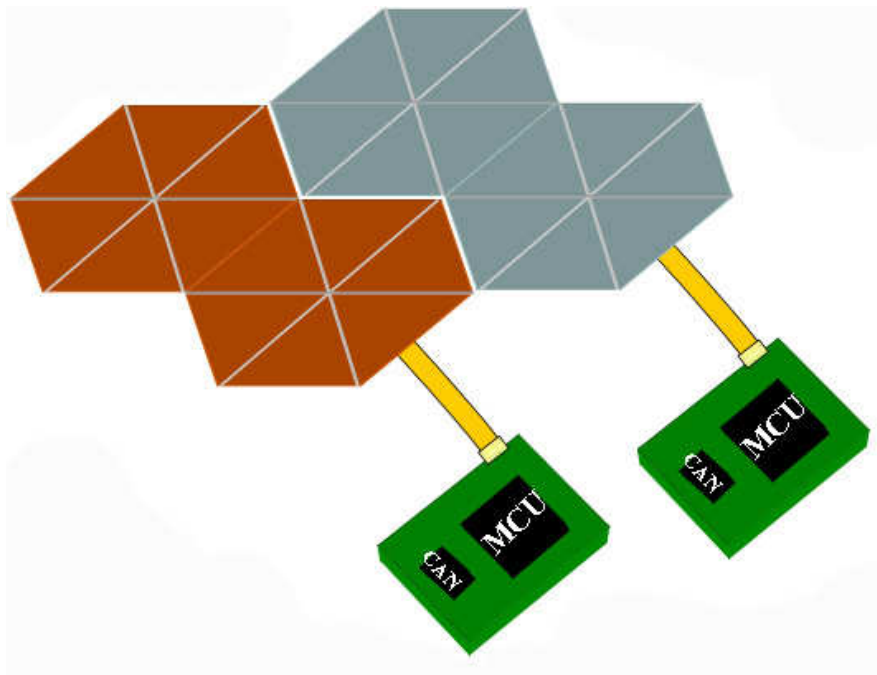
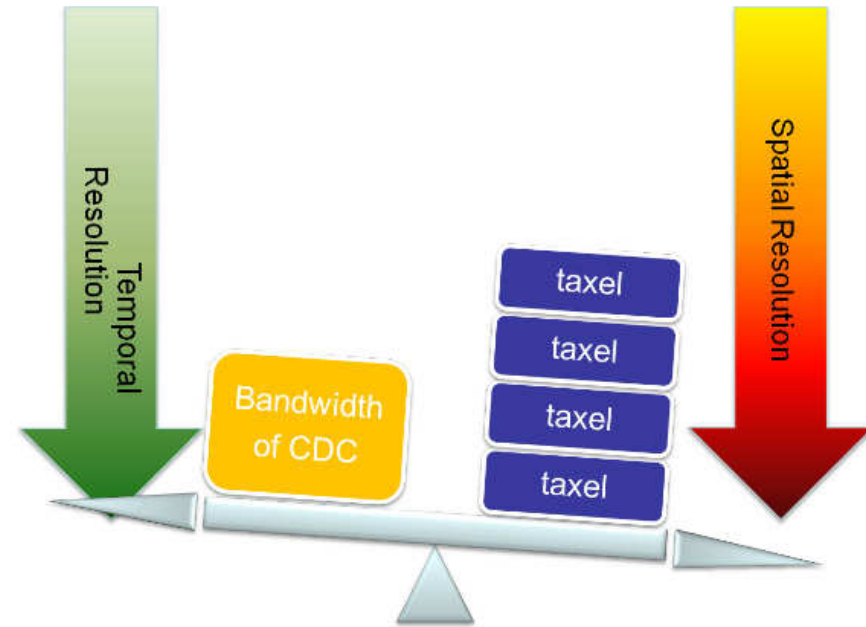


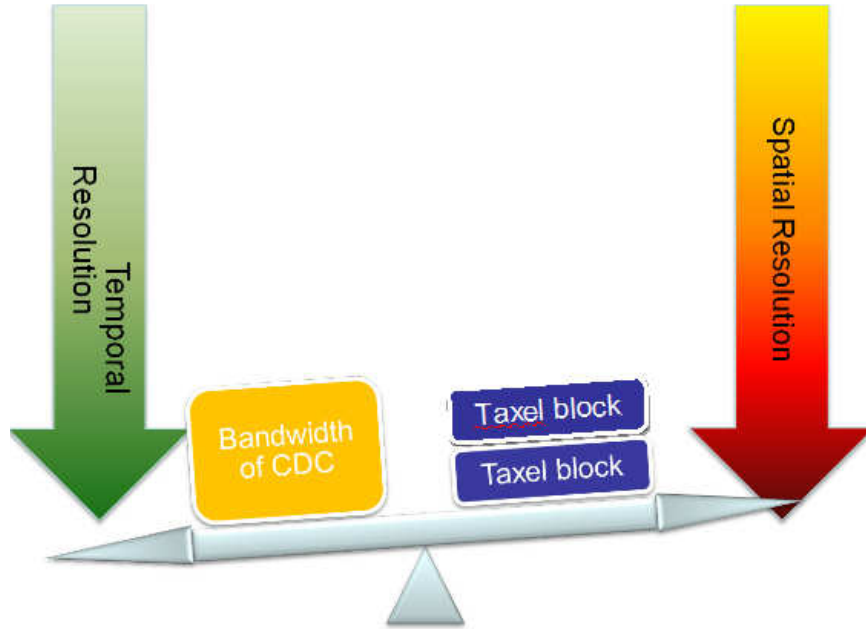
Figure 4.8: System Architecture. Many mesh of triangles can be put side by side in order to cover a wider surface

the spatial and temporal resolution. The second is in the processing of the data once they are acquired from the MCU, that means, from the MCU boards to the central PC. For the level two, we can use the techniques discussed on 3.1.5. While, for the first level, from the triangles and the MCU, the data processing techniques is based on feature of the CDC that we are using. The CDC indeed has 12 conversion stages (Device (2008)). In any stages it reads a capacitance (it takes 0.768, 1.536 or 3ms depending on the oversampling ratio), but subsequently the capacitance for any stage can be defined either as the single electrode (in the triangle module we have 12 electrodes) or as the sum of two or more electrodes (the maximum number is due to the fact that the total capacitance for each stage must be less then 30 pF). Therefore it is possible for example to reduce the spatial resolution, from 12 points each triangle to 3 macro areas each triangle, by increasing the temporal resolution from 18.4ms (9.2, 18.4 or 36.8ms depending on the oversampling ratio) to 4.6ms (2.3, 4.6 or 9.2ms depending on the oversampling ratio) or connect all the twelve point and read it faster (0.768, 1.536 or 3ms). These characteristic of the sensor system can be very useful for implementing control strategy where the sampling rate and resolution are changed dynamically. For example, when the robot has to avoid contact of its arm and the environment, it is important to have an high temporal resolution while the spatial one is less important. While, during exploration task it is important to have the contact shape, therefore the spatial resolution could be increased, reducing the temporal one, figure 4.9.

4. ARTIFICIAL SKIN: PROPOSED DESIGN



(a)



(b)

Figure 4.9: CDC could read back each taxel for the maximum spatial resolution (a) or blocks of taxels augmenting the temporal resolution (b)

Chapter 5

Simulations

5.1 Introduction

A capacitive sensor is basically a variable capacitor, therefore it is important to study its geometrical and physical properties in order to define the specifications for the design of the printed circuit board. Figure 5.1 shows the 16 bit linear response of the selected CDC (Device (2008)) with respect to the capacitance input in a range between 4 and 30 pF. It means that the only constrain, it regards the range of the capacitance, but the sensitivity is linear in the whole range (5.1). The simulations address the problem of characterizing the *ideal* capacitor, in function of: thickness of the dielectric material, area of the plate and dielectric constant of the material. The goal of the simulations is to find a capacitor that varies its capacitance inside of the CDC range (10-12 bits of the CDC span), with a good sensitivity and the smallest area possible (in order to maximize the spatial resolution). The maximum thickness of the material is fixed to $3mm$.

5.2 Variable Capacitor Characterization

For the characterization of the capacitor there are 3 parameters: dielectric permittivity, plate area and range of thickness of the dielectric material. The thickness of the material it is chosen to be in between $10\mu m$ and $3mm$. It has been chosen to vary the area from $10mm^2$ up to $50mm^2$. The dielectric material could be

5. SIMULATIONS

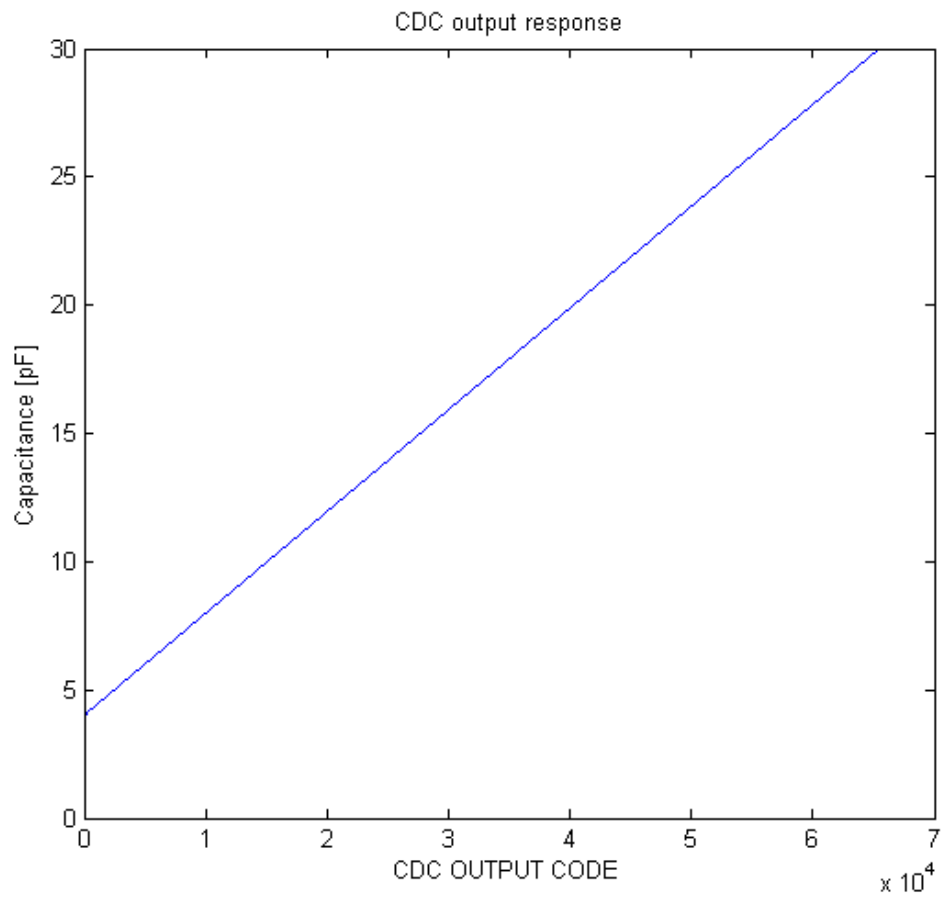


Figure 5.1: Characteristic of the CDC. It has been chosen a linear characteristic without considering the non linearity of the CDC (see AD7147 data sheet for more details)

5.2 Variable Capacitor Characterization

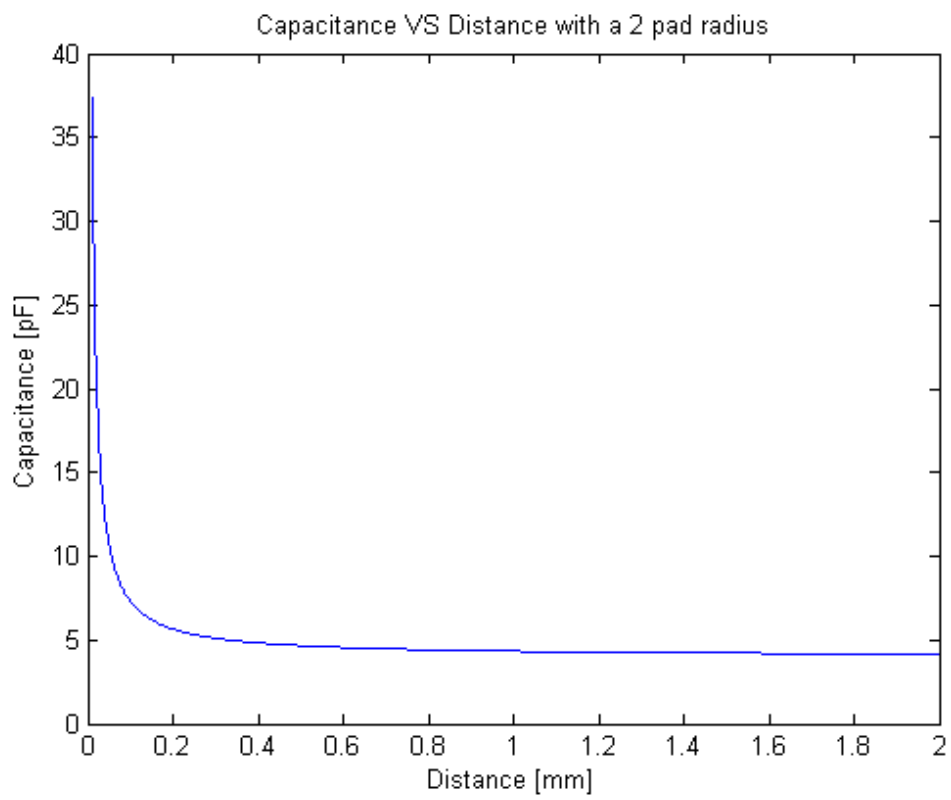


Figure 5.2: Capacitance VS Distance curve for a capacitor with plates of 2mm radius

5. SIMULATIONS

used for the soft layer are urethane foam, silicone rubber foam and neoprene. Therefore the range of variation of the dielectric constant is from 3 to 7, staying at what is reported in the literature. However, since the deformation of the material changes both the thickness and the density, the dielectric constant could also change.

5.2.1 Capacitance VS Area

The capacitance is proportional with respect to the area of the capacitor plates. In the plot 5.3 is shown how the response of the sensor changes with respect to the area, considering areas from 10mm^2 to 50mm^2 .

$$\frac{dC}{dA} = \frac{\varepsilon_0\varepsilon}{x} \quad (5.1)$$

5.2.2 Capacitance VS Dielectric Constant

The capacitance is proportional with respect to the dielectric constant of the soft material. In the plots below is shown how the response of the sensor changes with respect to the dielectric constant from 1 to 7;

5.2.3 Capacitance VS Variable Relative Permittivity

The deformation of a soft material, like urethane foam or neoprene, changes the density of the material and consequently its relative permittivity. It has been considered an *ideal* material, who changes linearly its permittivity with respect to the thickness.

5.3 Discussion

The simulations shows how to change the sensitivity of the transducer changing both the geometry of the sensor (area of the pads and thickness of the dielectric material) and the permittivity of the material . The bigger the area, the higher the sensitivity. A similar result there is for the permittivity, the higher the permittivity the higher the sensor response. However another important parameter

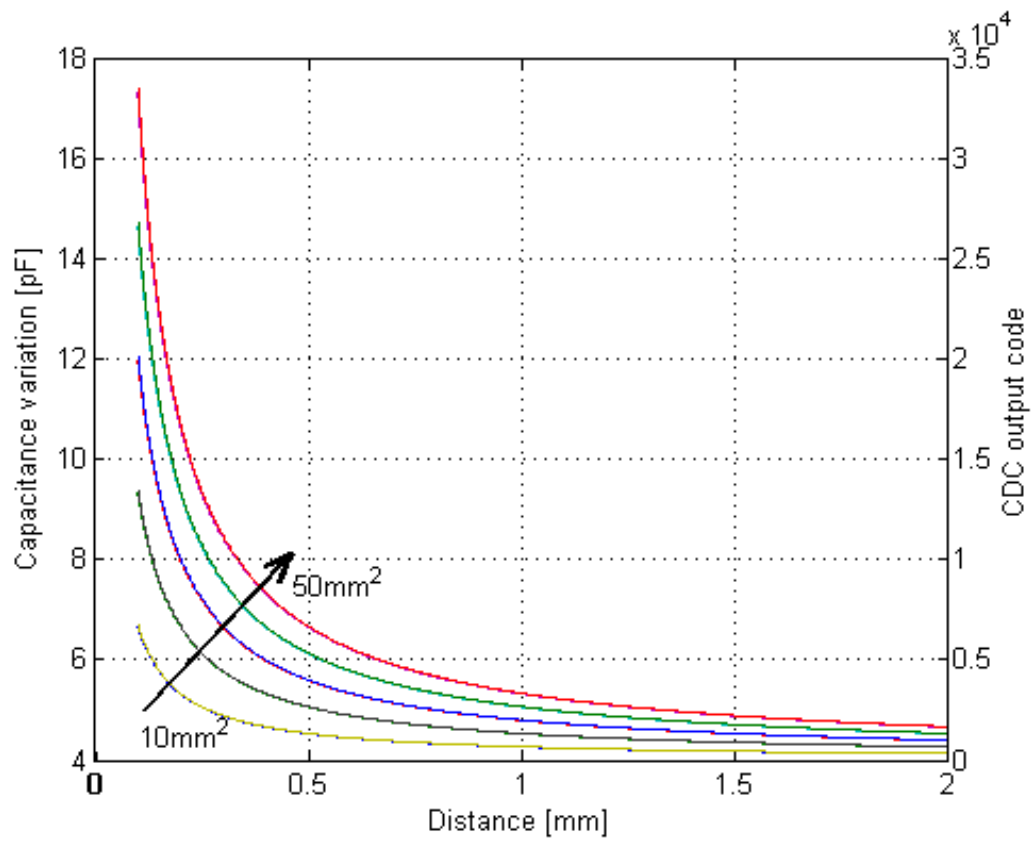


Figure 5.3: Capacitance and CDC output VS Area for a capacitor with plates from 10mm^2 to 50mm^2

5. SIMULATIONS

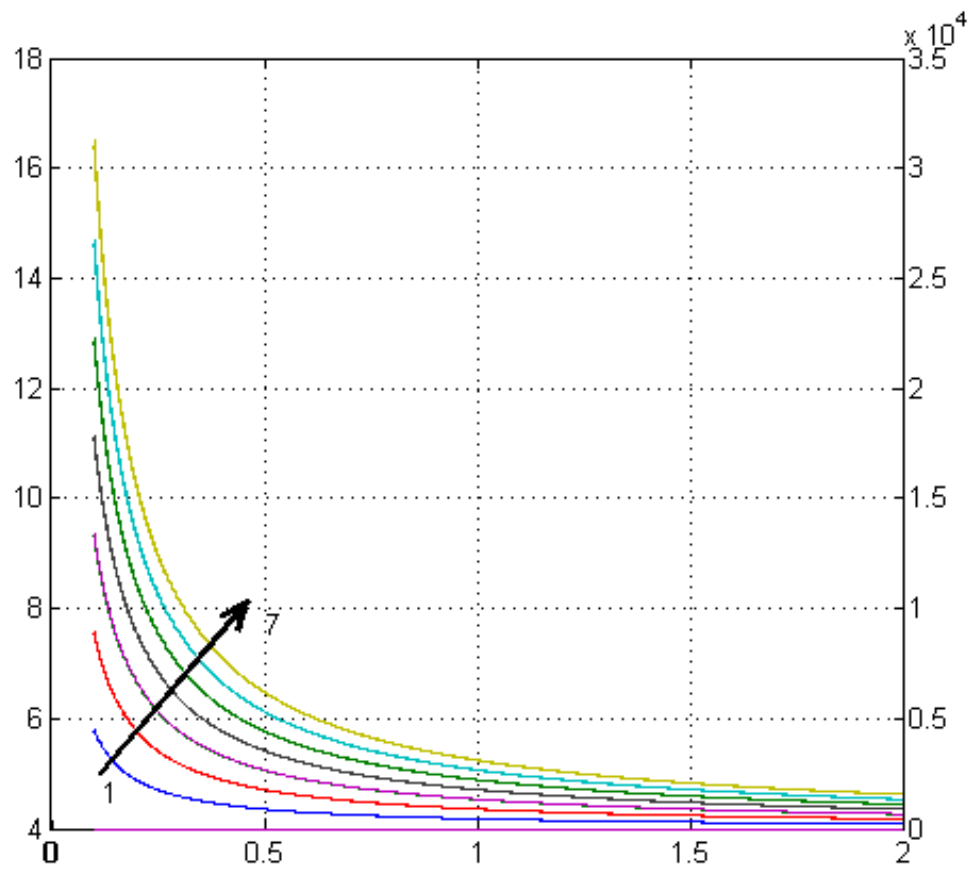


Figure 5.4: Capacitance and CDC output VS Distance curves for materials with dielectric constant from 1 to 7

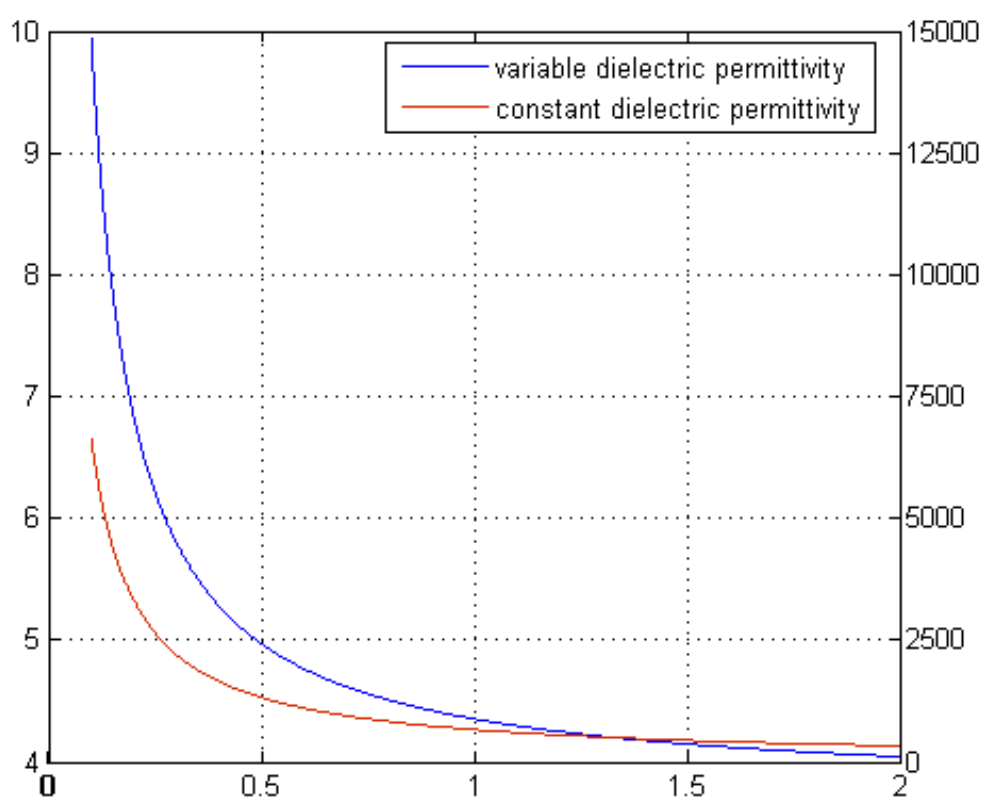


Figure 5.5: Capacitance VS Distance curve for materials either constant permittivity of 3 and variable permittivity from 1 to 7

5. SIMULATIONS

is the Young's module of the material, which determines the pressure required to reduce the thickness of the dielectric of a certain amount. A trade-off between all these parameters is required in order to achieve the sensor sensitivity and range of pressure we want to measure. Therefore it is possible to adapt the sensor response in order to adapt it to the different parts of the robot's body.

Chapter 6

Design of a prototype

6.1 Introduction

After the analysis by simulation, prototypes of the whole system have been designed and built. The project concerns the design of the electronic boards: schematic, layout and choice of the components, the development of the firmware for the microcontroller and software for the visualization of the taxels responses. In the next sections a detailed description of each module is presented. Furthermore in section 6.5 the entire process for producing a mesh of tactile sensors is described. Section 6.5.2 shows an example of how to install the artificial skin on the humanoid robot iCub.

6.2 Triangle Module

As mentioned in chapter 4 the idea of using a mesh of triangles for covering three dimensional surfaces is inspired by the triangulation technique, widely used in computer graphics. Using triangles in fact, it is possible to approximate complex surfaces (such as the outer shell of a humanoid robot), for example, in the arms, legs and chest. The triangle is the base unit of the proposed tactile sensor. It consists of an off-the-shelf CDC (AD7147 from Analog Device in the present implementation, Device (2008)) that provides twelve 16 bit measurements of capacitance. The sensor has three communication ports placed along its sides: one

6. DESIGN OF A PROTOTYPE

for the input from an adjacent triangle, and the other two as outputs toward adjacent triangles. The support of the sensor is a four layer flexible PCB. In the top layer 12 circular pads are etched, forming the taxels, acting as plates of capacitors. On the other side of the PCB the CDC chip is mounted and the three communication ports are etched, as shown in figure 6.1 and 6.2. Moreover, on the top layer there is a thick silicon rubber foam layer and a thin ground plane on top of it. The ground layer acts as the other plates of the capacitor for the 12 pads.

The triangles are interconnected through the communication ports on the PCB, without using additional cables. The communication ports have 7 pins: 2 for the power supply and five for the 4 parallel **Inter Integrated Circuit** buses (I2C). There is a common clock line (SCLK) and four data lines (SDA). It is possible to connect up to 16 triangles in the current implementation (figure 6.3). A single cable goes from the mesh to the microcontroller, reducing the problem of wire management. In the first prototype all the triangles are equal in shape and dimension, but it is possible to change the size and the shape in order to better approximate complex surfaces. However the flexibility of the triangle itself gives an advantage in terms of conformability with respect to computer graphics technique where the triangles are considered to be rigid.

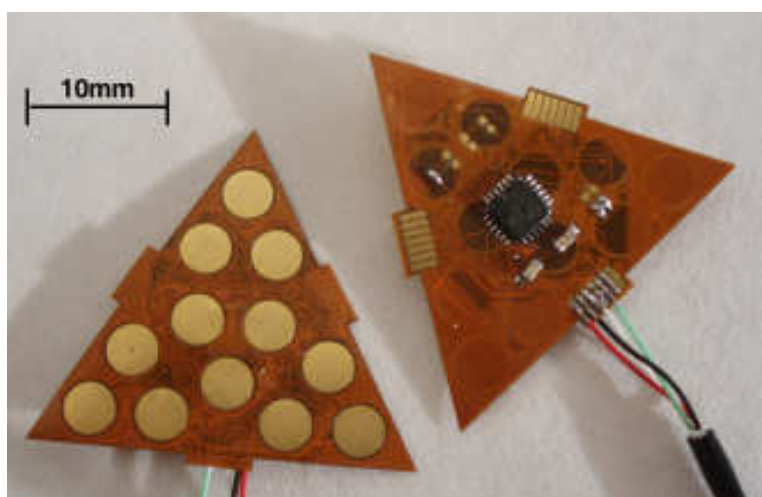


Figure 6.1: The triangle module. Each sensor implements 12 taxels and hosts the capacitive transduction electronics.

6.2 Triangle Module

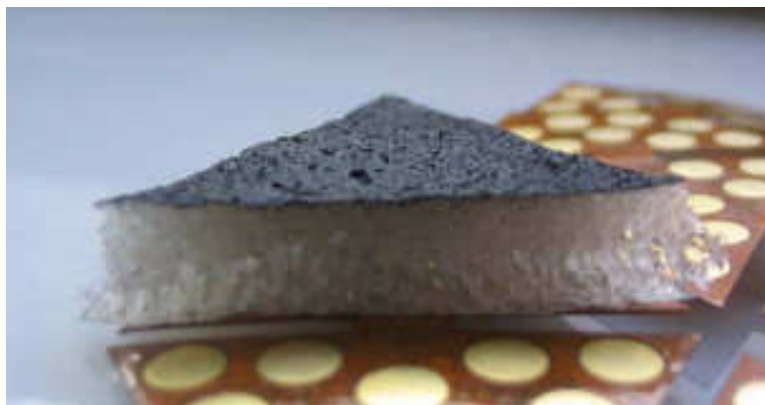


Figure 6.2: The thick layer of silicone rubber foam covering the sensors and the conductive layer used as ground plane sprayed on top.

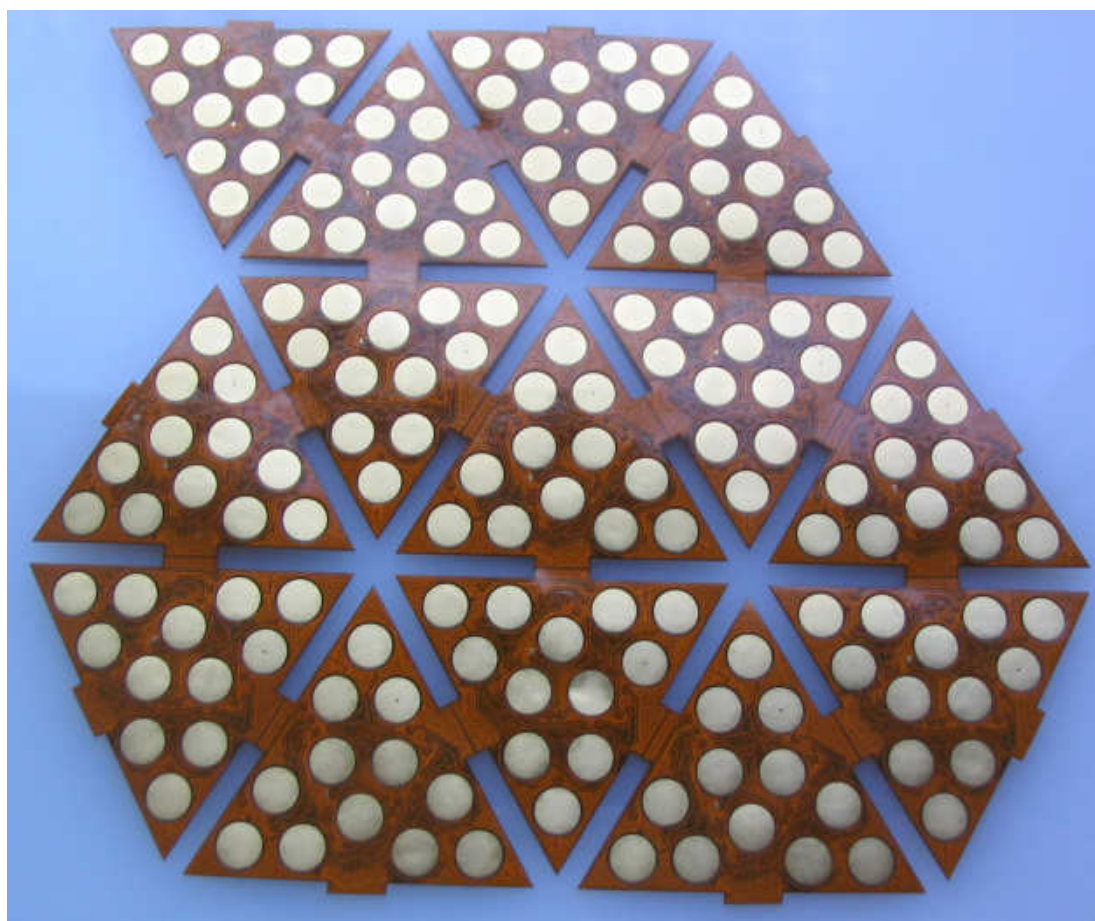


Figure 6.3: 16 triangles interconnected on a flexible PCB

6.3 Microcontroller Board

The microcontroller board (figure 6.4) is used for programming the CDCs, driving the taxels and for reading the pressure measurements. The microcontroller (dsPic30F4011 from Microchip, Microchip (2008)) can also be used to switch to different readout modes. In fact, it is possible to program the CDC in order to get either average measurements of the taxels at high frequency (up to 500 Hz), or reading the 12 measurements independently at a lower frequency up to 50 Hz. Furthermore, it is possible to implement algorithms in order to process the raw pressure data and compress them, or to start firing (like in the human) only when a stimulus has occurred. The features of the microcontroller boards are summarized below:

- dsPic30F4011 20MIPS microcontroller
- 8MHz external oscillator
- CANbus transceiver or RS232 point to point link
- Four parallel I2C buses (1 SCK and 4 SDA) to connect up to 16 triangles.

Furthermore functions of the MCU module are:

- To configure the triangles
- Calibration of the triangles at the start-up.
- Data processing
- To send the data coming from the triangles to a PC through the CAN-bus or an RS232 link

The modularity of the system provides the opportunity of changing the MCU module for example for either increasing the bandwidth of the bus, or the computational power, without changing the entire system. *Flexray* automotive bus with a bandwidth of 10Mbit/s or *Ethercat* may become available in the future.

6. DESIGN OF A PROTOTYPE

6.4 Software for Data Acquisition

The software for data acquisition has been implemented in Matlab, in order to have the maximum flexibility and the possibility to elaborate data after acquisition. In order to connect the CANbus link of the MCU board to a PC, a USB-CAN converter was used (ESD-CAN from ESD-Electronics). Therefore, a Simulink blocks library (figure 6.5) has been developed, implementing reading and writing functions from the ESD-CAN converter. The simulink model (figure 6.6) reads the CAN messages (for protocol specification see A) and plots and save them for post processing.

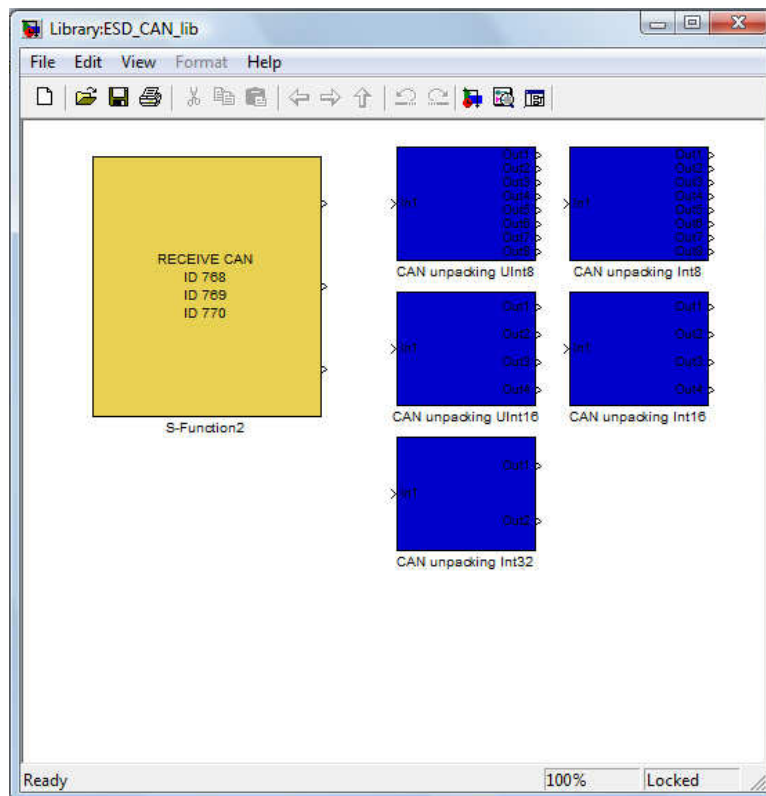


Figure 6.5: Library Blocks for the ESD-CAN usb to CAN converter in Simulink

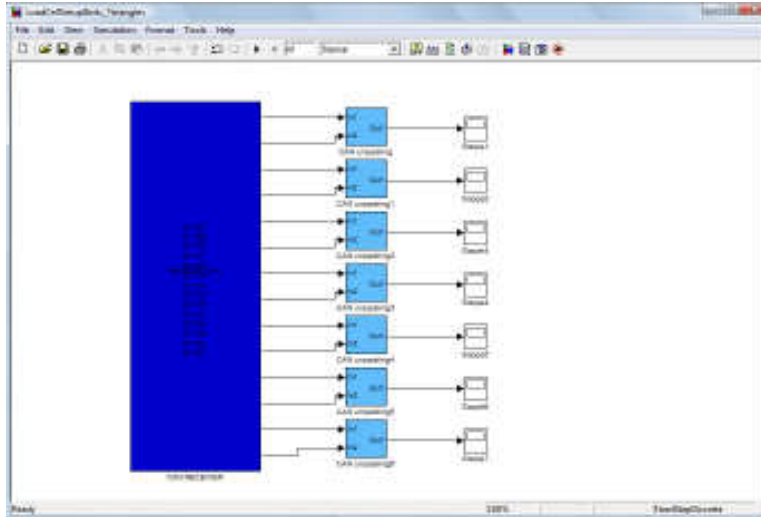


Figure 6.6: Simulink Model for reading the triangles modules

6.5 Hexagon prototype

In this section the fabrication process of a prototype with six triangles in an hexagon configuration is described . The prototype has been embedded in a silicone rubber foam, and it has been covered by a conductive fabric acting as a ground plane (see 4.2). After soldering the components on the flexible PCB, the board is inserted on a PTFE mold with the electrodes side turned towards the bottom of the mold (figure 6.7). Then the mold is poured with silicone rubber foam (Soma Foama 15 from Smooth-on). In this way, a thin layer of silicone rubber covers and protects the electronics (figure 6.8). After the curing time of one hour, the PCB is turned by 180 degrees and placed again in the mold (figure 6.9). It is poured with silicone rubber foam in order to create the dielectric of the capacitors (the soft layer). After the curing time, a conductive fabric is glued on the top of the soft layer and is connected to the ground of the PCB.

6.5.1 Prototype on a 3D curved surface

In order to test the conformability of the skin over a 3D surface the hexagon prototype has been installed on a solid object that can be considered as a dummy cover of the robot. After embedding the skin on the silicone rubber, the patch

6. DESIGN OF A PROTOTYPE

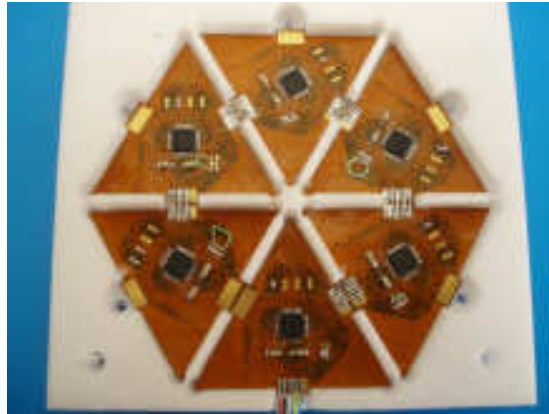


Figure 6.7: The board is inserted on a PTFE mold with the electrodes side turned towards the bottom of the mold

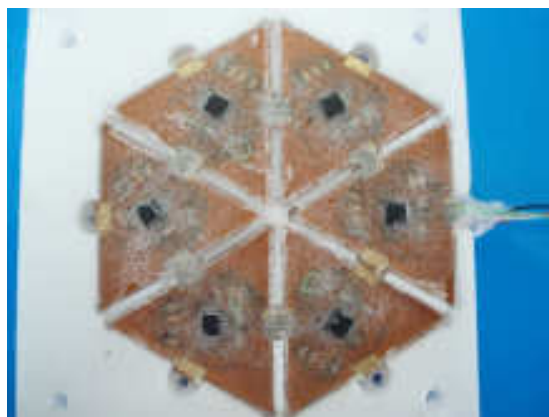


Figure 6.8: After the placing of the board the mold is poured with silicone rubber foam

6.5 Hexagon prototype

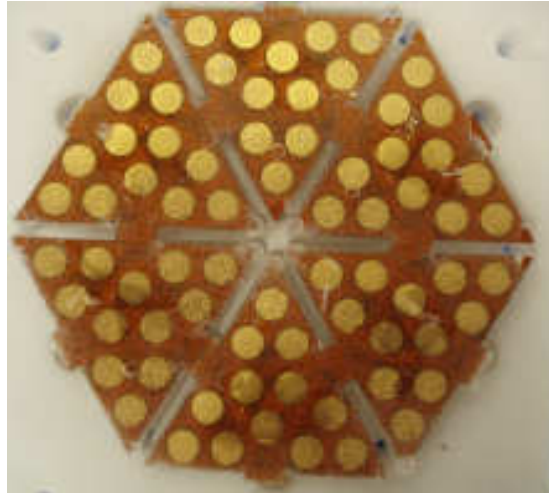


Figure 6.9: The board is turned 180 degrees



Figure 6.10: After the placing of the board the mold is poured with silicone rubber foam

6. DESIGN OF A PROTOTYPE

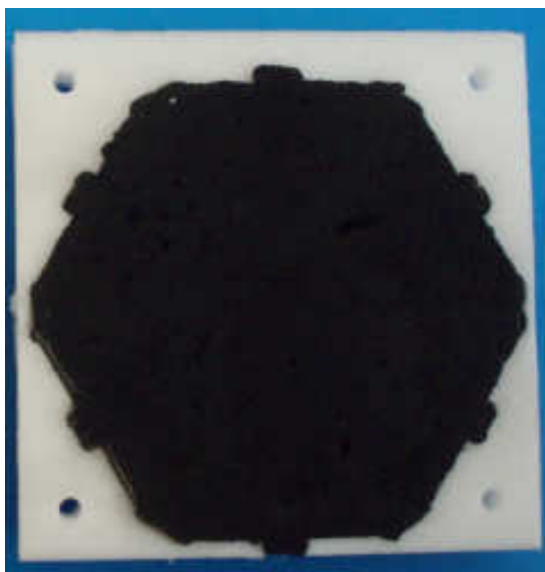


Figure 6.11: A conductive layer is glued on the surface of the sensor

has been glued on the curved object. The aim of the experiment was to test the conformability and the robustness of the sensors. Regarding the conformability we can say that it is possible to bend the sensor over a 3D surface. This property depends on the size and the shape of the triangles with respect to the solid to be covered. In order to achieve better results the triangular modules can be tailored to the specific application (curvature). There are not quantitative experiments on the robustness of the sensor. However once the sensor is bended and fixed on a surface the flexible PCB does not show any problem. The flexible PCB is fragile if you bend it many times, but once it is fixed on a surface it is stable over time.

6.5.2 Prototype on the iCub palm

In order to evaluate the sensor on the humanoid robot iCub, a first prototype to be mounted on the palm of the robot has been designed. To install and uninstall the skin quickly and conveniently, we have done a mold of the carbon fiber palm using multi-layer fiberglass (figure 6.13). Then, the triangles sheet has been cut in order to use only the triangles needed for covering the palm (figure 6.14). After having protected the electronics by means of silicone rubber, the triangles are

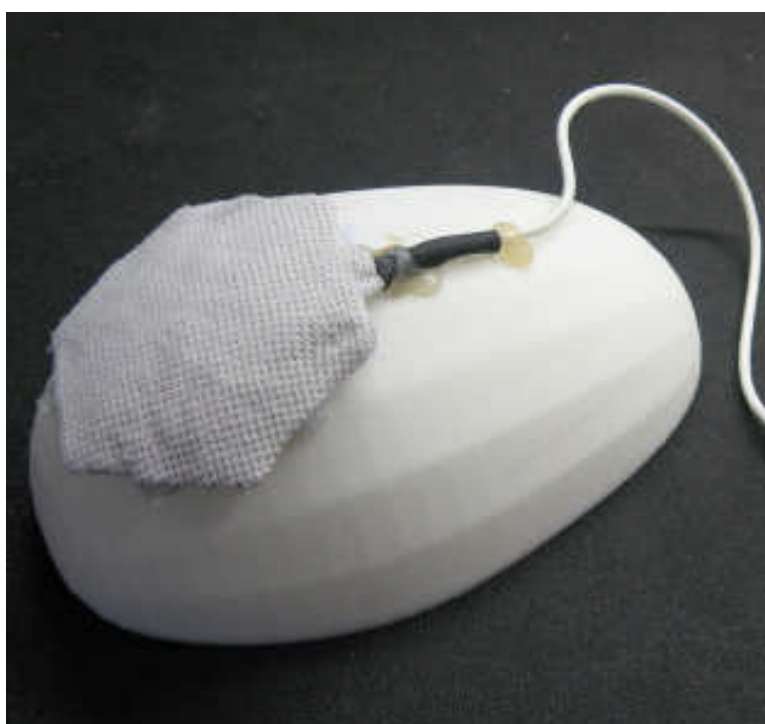


Figure 6.12: The hexagon has been installed on a 3D surface. The sensor can be curved to approximate the solid.

6. DESIGN OF A PROTOTYPE

glued on the mold, (figure 6.15). In this case the soft-layer is made of neoprene instead of silicone rubber as shown in (figure 6.16). The microcontroller board will be mounted on the forearm of the robot.

6.6 Skin Graphical User Interface

A graphical user interface has been realized in order to visualize the data coming from the artificial skin. The software is designed in *Visual C++ .NET* and it requires the *.NET Framework*. A RS232 is used for communication from the MCU module and the PC. The software provides a visualization of the taxels representing the pressure with a colormap that goes from black to yellow. The more yellow the more pressure exert on the taxel.

6.6 Skin Graphical User Interface



(a)



(b)

Figure 6.13: Multi-layer fiberglass mold and the carbon fiber palm of the robot (a). The mold fits the palm and can be placed and removed (b)

6. DESIGN OF A PROTOTYPE

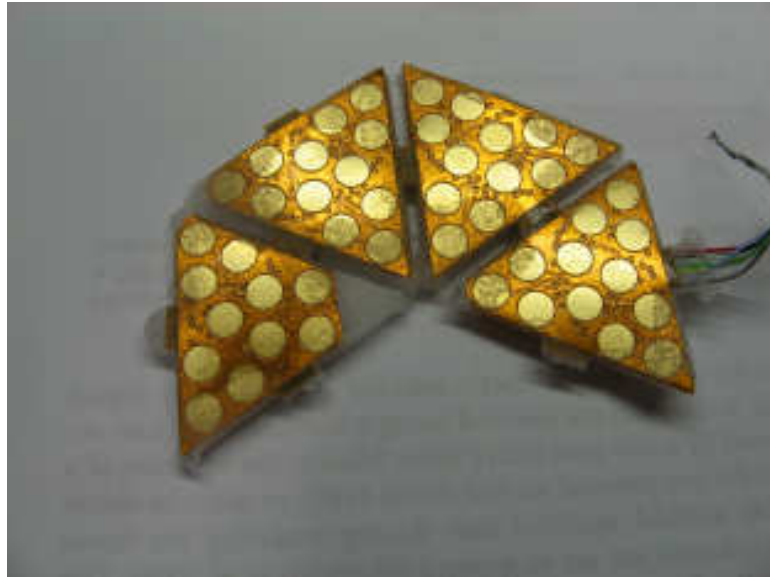


Figure 6.14: From the triangle sheets, four triangles are cut in order to fit on the palm.



Figure 6.15: The triangles are glued on the fiberglass mold.

6.6 Skin Graphical User Interface



(a)



(b)

Figure 6.16: The sensor is mounted on the palm (a). It is covered by a 1mm thick neoprene and a conductive fabric acts as the ground plane(b)

6. DESIGN OF A PROTOTYPE

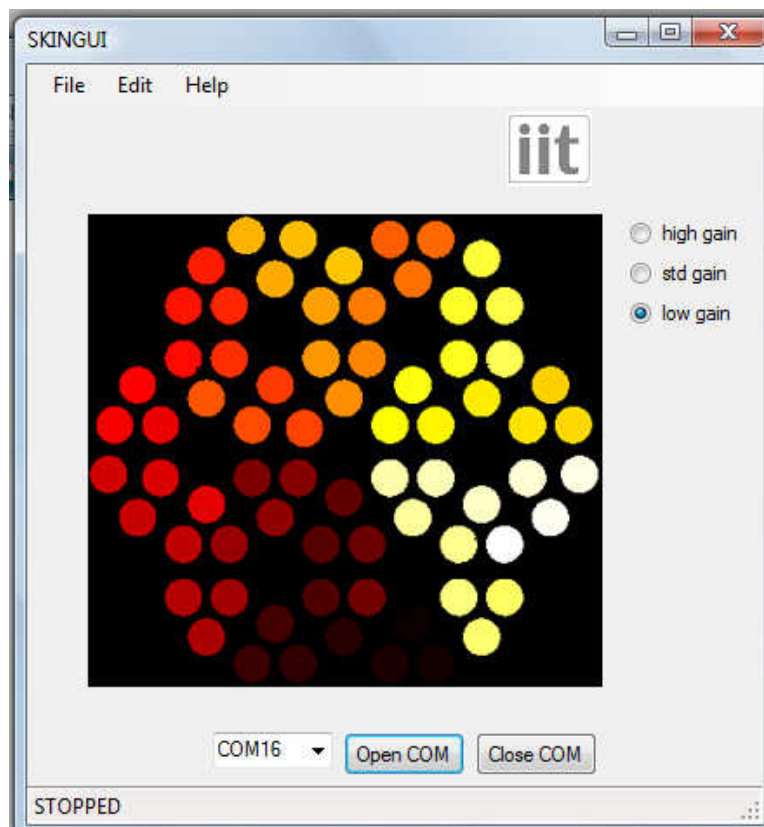


Figure 6.17: SKINGUI is a software to visualize the skin output. A colormap is used to represent the pressure exert on each taxel

Chapter 7

Experiments

7.1 Introduction

Experimental tests has been carried out in order to characterized the sensor response. As discuss in chapter 5, we expected that the properties of the sensor depends mainly by the physical properties. Therefore it is possible to change the behavior of the sensor, changing the material properties. However the goal of these experiments is not to find the best solution in term of material, but to prove the reliability of the sensor and to show its main characteristics.

7.2 Experimental Setup

We used an off-center load cell (3 kg AL series, from Laumas2) suitable to measure static forces. Pressure is applied with a micrometer (TESA Micromaster IP54) by moving a metal probe vertically against the sensor. The micrometer position can also be monitored. When it is moved downward, it applies pressure to the triangular module (see figure 7.1). The triangle is mounted on the load cell, (figure 7.1). A 10 bits strain gage amplifier (Precision Instruments AT-10) and an analog to digital converter input in the MCU module has been used to get the signal from the loadcell. A CAN-USB interface (ESD-CAN) has been used to collect data from both the triangle and the loadcell.

7. EXPERIMENTS



Figure 7.1: Test setup with a load cell that can measure static forces. The off-center load cell (3 kg AL series, from Laumas) and the micrometer (TESA Micromaster IP54) are shown

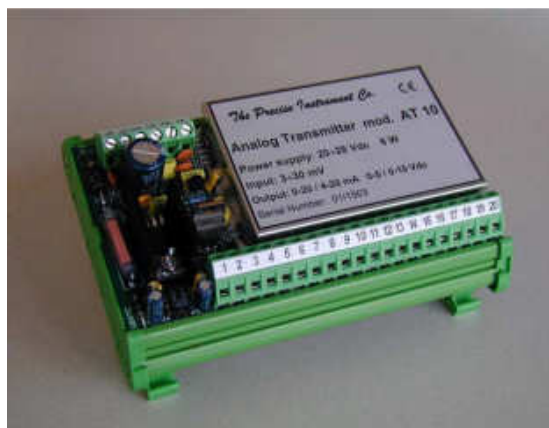


Figure 7.2: The strain gage amplifier used for the loadcell (Precise Instrument AT-10).

7.3 Experiments on a triangle module

The main experiment activity has been carried out on a single triangle module. The first set of experiments has been carried out using the setup described above and installing a circular probe with the radius of $12mm$ on the micrometer, positioned in the center of the triangle (figure 7.3). Therefore we expect to have the three pads under the probe with an higher change in the capacitance, the 6 closed to three with a medium response and the three in the angles of the triangle with a small response. The second set of experiments is analogous with the previous one, but instead of reading independently the twelve measurements, we set up the triangle to read either three or one macro-areas. In the third set of tests, we have installed on the micrometer a probe with the surface bigger then the triangle in order to press the whole triangle uniformly. The material used for these experiments as soft layer is silicone rubber Soma Foam 15 from Smooth-on. The thickness of the layer is 3mm. On top of the rubber a thin conductive fabric is glued on it. Finally we have changed the soft layer, using 1mm of neoprene instead of the silicone rubber in order to show how it is possible to change the measurements range of the sensor, without modifying the electronic.

7.3.1 First Experiment: Sensor Response with a 12mm probe

The first set of experiments has been carried out using the setup described above and installing a circular probe with the radius of $12mm$ on the micrometer, positioned in the center of the triangle(figure 7.3).

7.3.1.1 Static Response

The static response experiment is a load-unload cycle where a pressure is applied and released. At any step of the experiment we move the probe down of $0.1mm$ and then we start recording data, therefore we eliminate the transient response. Figure 7.4 shows the behavior of the twelve pads. As we expected, the pad under the probe (blue traces) have the higher response; the black traces represents the six neighbors and finally the three pads in the angles are in red. We were

7. EXPERIMENTS

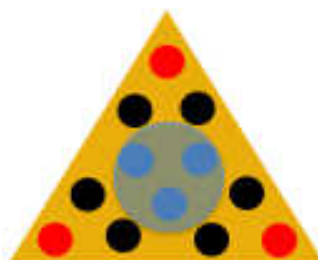


Figure 7.3: The circle represents the probe of the pressure. The central pads in blue are under the probe, the six in black are the one closed to the probe and the three in red in the angles are far from the probe.

expected no response from them, however a slightly change is visible that is due to the deformation of the silicon rubber foam due to the stress in the middle.

Using the data coming from the loadcell the curve of the sensor with respect to the pressure has been sketched in figure 7.5.

Reading from the panel of the micrometer the depth (change of 0.1 mm every cycle) of the probe it was also possible to build the characteristic of the taxels with respect to the deformation of the soft-layer.

In figure 7.7 is shown the characteristic curve of the loadcell with respect to the indentation. As you can see, there is an hysteresis that causes a big error in the characterization of the tactile sensor itself, and it is mainly due to the loadcell, and this is easy to see comparing figure 7.6 with figure 7.7.

7.3.1.2 Low Frequency Response

The low frequency response of the sensor is evaluated increasing and releasing a certain amount of pressure during recording of the data. Figure 7.8 shows the output of the taxels during the experiment, and in figure 7.9 shows the characteristic pressure versus response of the sensor. Even in this case we can observe the behavior of the three groups of pads. It was not possible to read the position of the probe during these experiments because the micrometer does not have any serial connection to the pc, therefore only in static conditions it is possible to record the position by hand.

7.3 Experiments on a triangle module

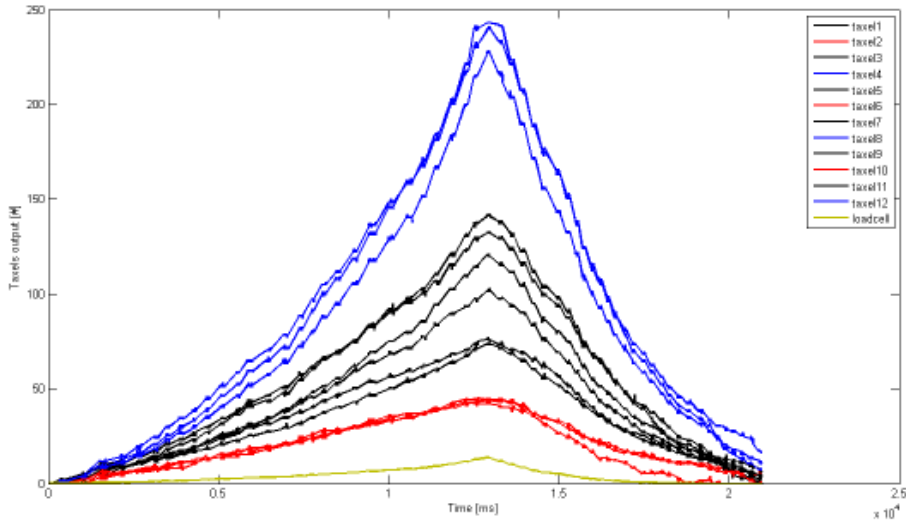


Figure 7.4: A load/unload cycle, with a 12mm probe on the center of the triangle. As you can see there are three taxels with an higher response (the three under the probe), 6 with a small response (the neighbors) and 3 representing the angles of the triangle where the signal is stable.

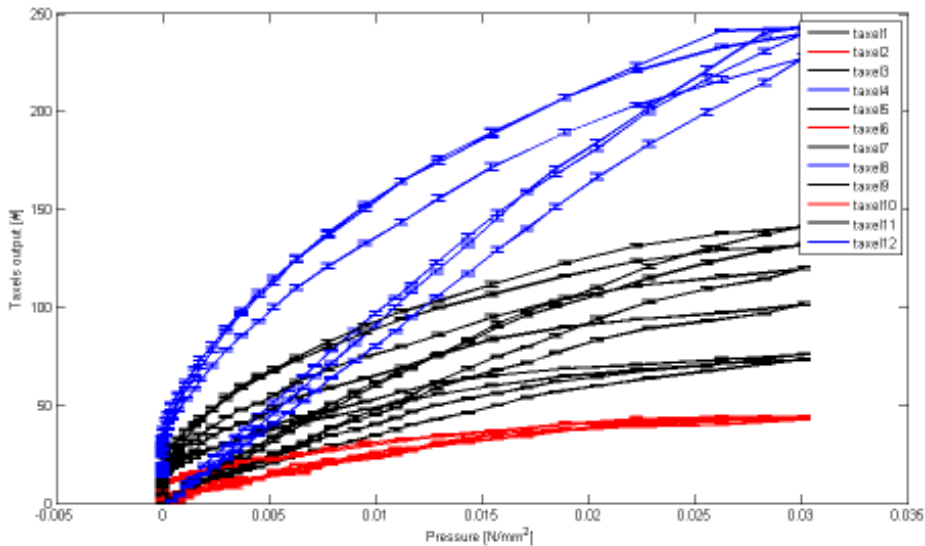


Figure 7.5: Taxels versus Loadcell characteristic.

7. EXPERIMENTS

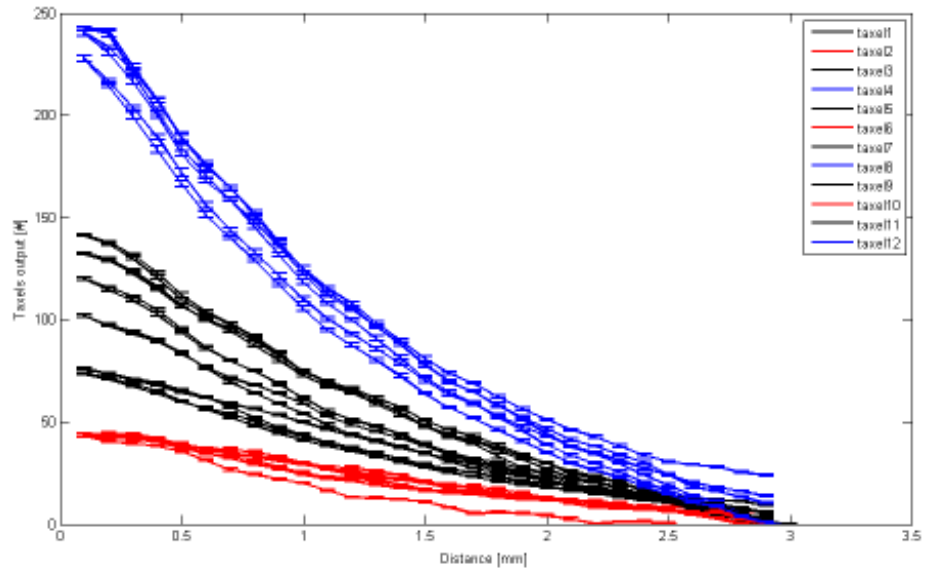


Figure 7.6: Taxels versus Deformation characteristic. As you can see the hysteresis here is much less than in figure 7.5, that means that part of the hysteresis is due to the loadcell as shown in figure 7.7.

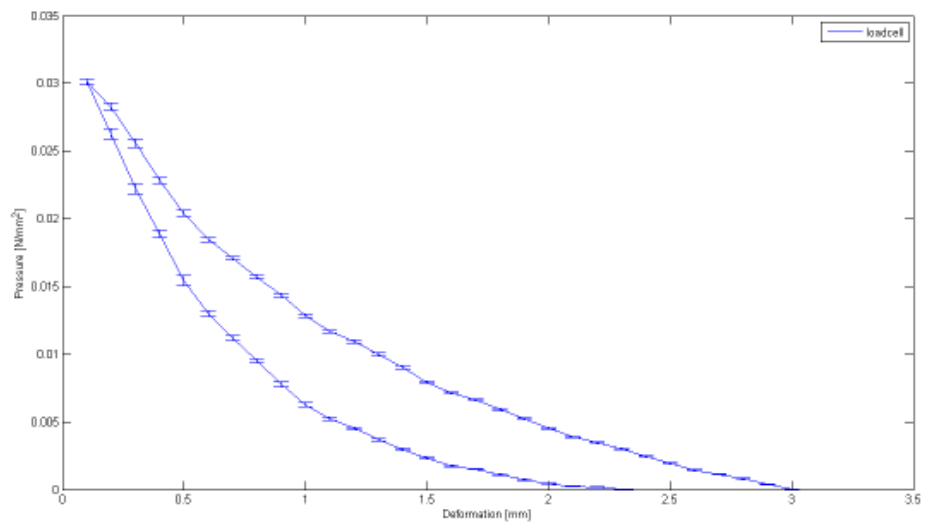


Figure 7.7: The hysteresis of the load cell during a static load and unload cycle. It is clear how big it is with respect to the one of the sensor (figure 7.6).

7.3 Experiments on a triangle module

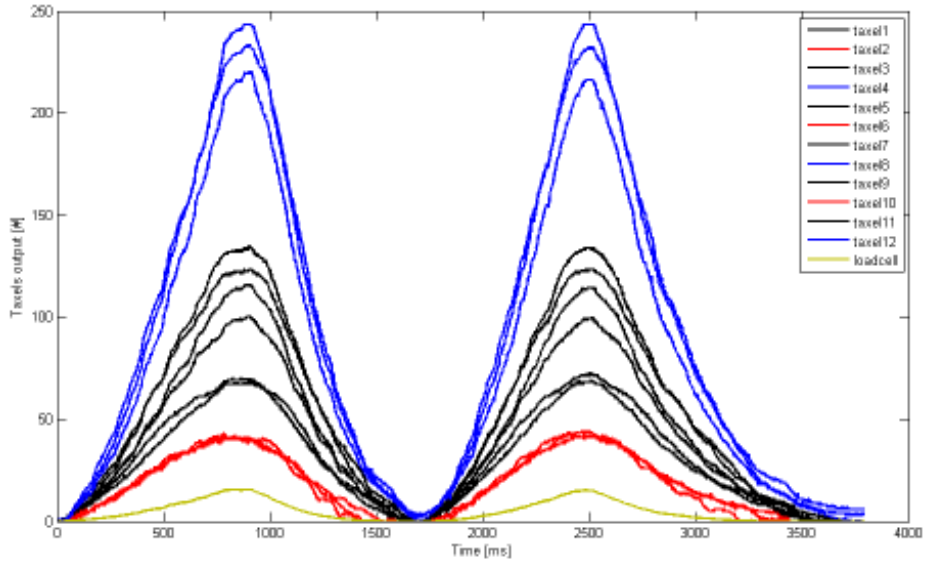


Figure 7.8: Two load and unload cycles.

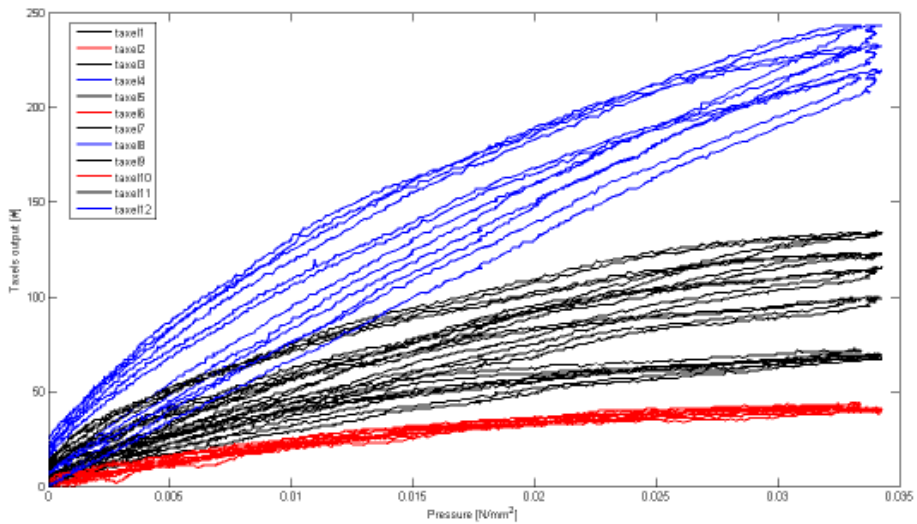


Figure 7.9: Taxels versus Loadcell characteristic.

7. EXPERIMENTS

7.3.2 Second Experiment: Sensor Response with a 12mm probe reading macro-areas

As discuss in chapter 4, the sensor has the possibility of reading groups of taxels that we call macro-areas. Reading macro-areas we increase the sensitivity of the sensor and we speed-up the time response of it. We decided to read either 3 areas of 4 pads each or the all 12 pads as a single area. Even in this case we carried out static and dynamic experiments in order to show sensor response and characteristic with respect to pressure and deformation.

7.3.2.1 Static Response

The static experiments are carried out as in section 7.3.1.1. Figure 7.10 graphs the characteristic curve sensor output versus pressure, while figure 7.11 shows the sensor versus deformation characteristic.

A second set of experiments has been done reading just one macro-area composed by the 12 taxels. Results are reported in figures 7.12 and 7.13.

7.3.2.2 Low Frequency Response

The dynamic experiments are carried out as in section 7.3.1.2. Figure 7.14 shows the sensor output, while the characteristic pressure versus sensor output is graphed in figure 7.15.

A second set of experiments has been done reading just one macro-area composed by the 12 taxels. Results are reported in figures 7.16 and 7.17.

7.4 Third Experiment: Sensor Response with a uniform pressure distribution

This set of experiments is carried out using a probe of the micrometer with a surface bigger then a triangle. In this way the pressure is approximately the same for all the 12 taxels (there is an error due to the uncertainties on the thickness of the two layers of silicon rubber foam above and under the flexible pcb), figure

7.4 Third Experiment: Sensor Response with a uniform pressure distribution

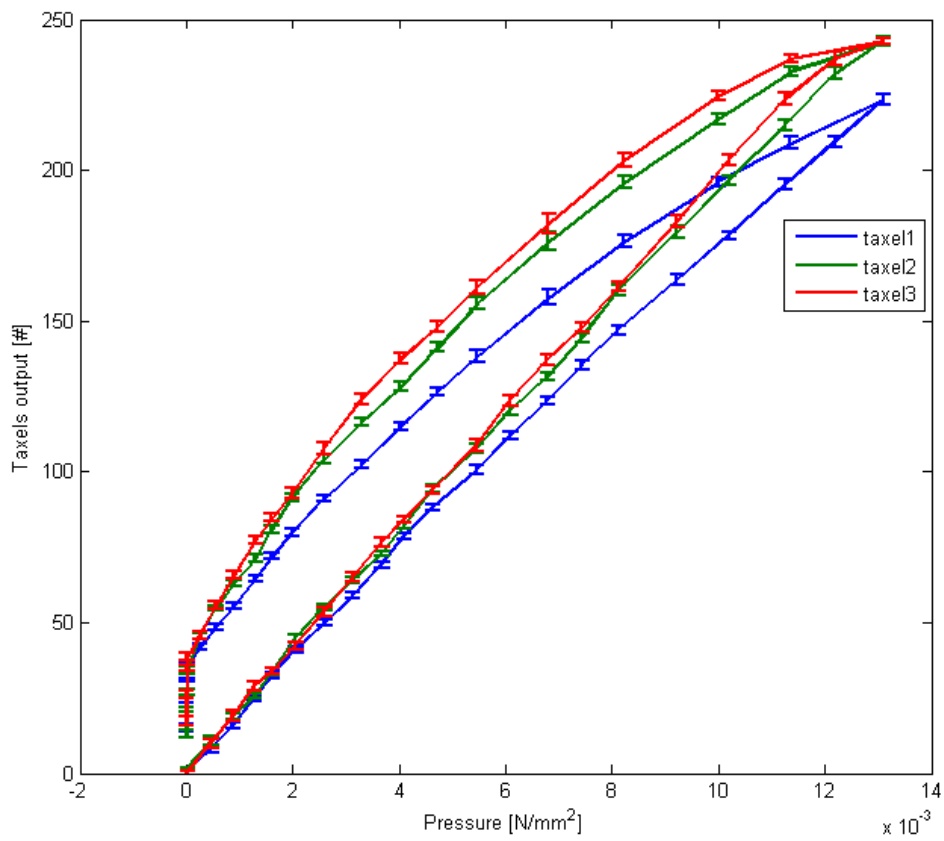


Figure 7.10: Taxels versus Loadcell characteristic of three macro-areas.

7. EXPERIMENTS

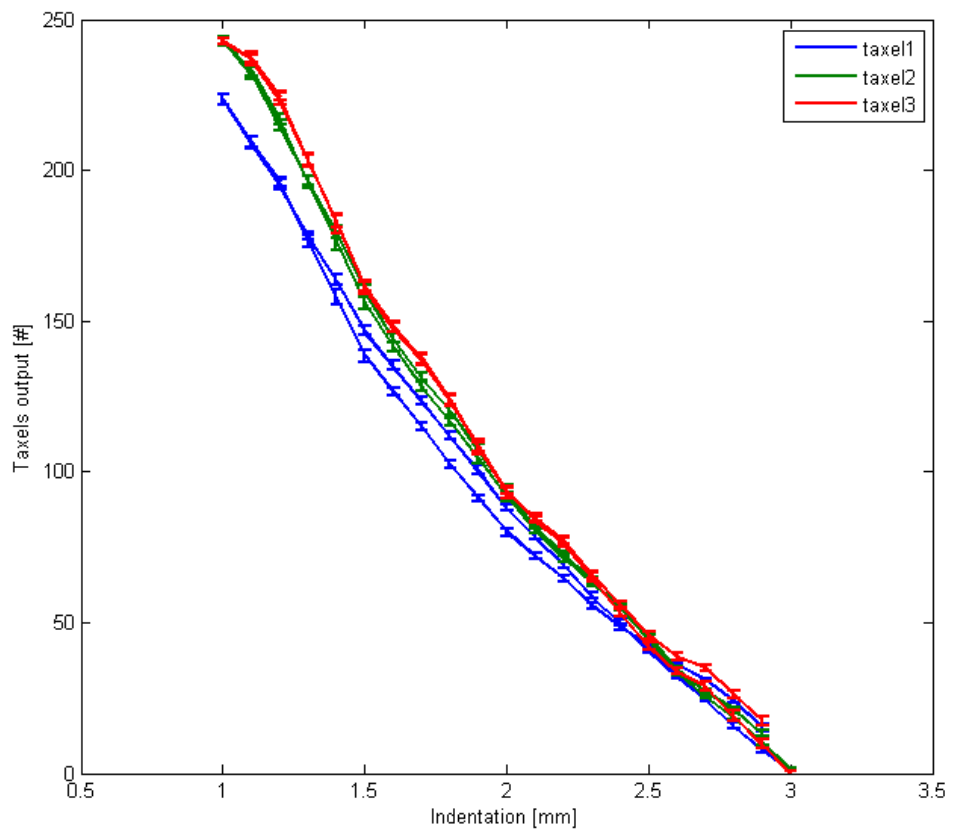


Figure 7.11: Taxels versus Deformation characteristic of three macro-areas

7.4 Third Experiment: Sensor Response with a uniform pressure distribution

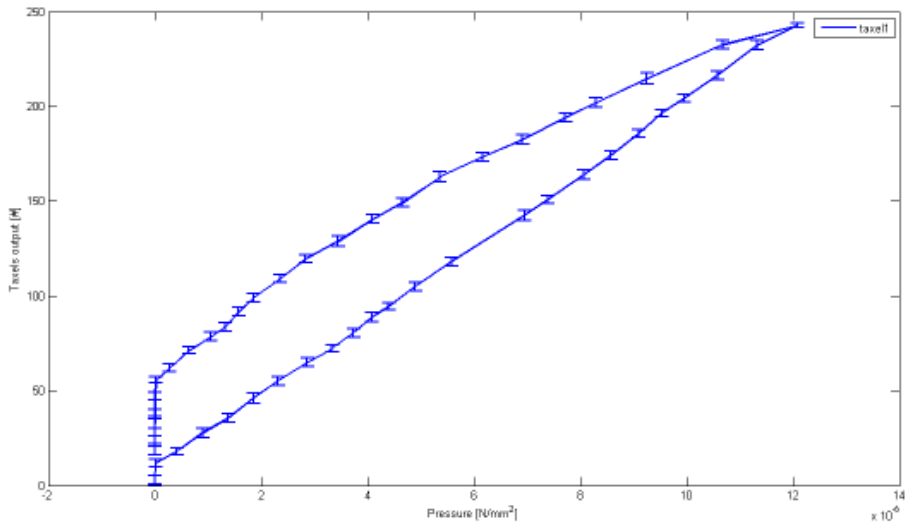


Figure 7.12: Taxels versus Loadcell characteristic of one macro-area.

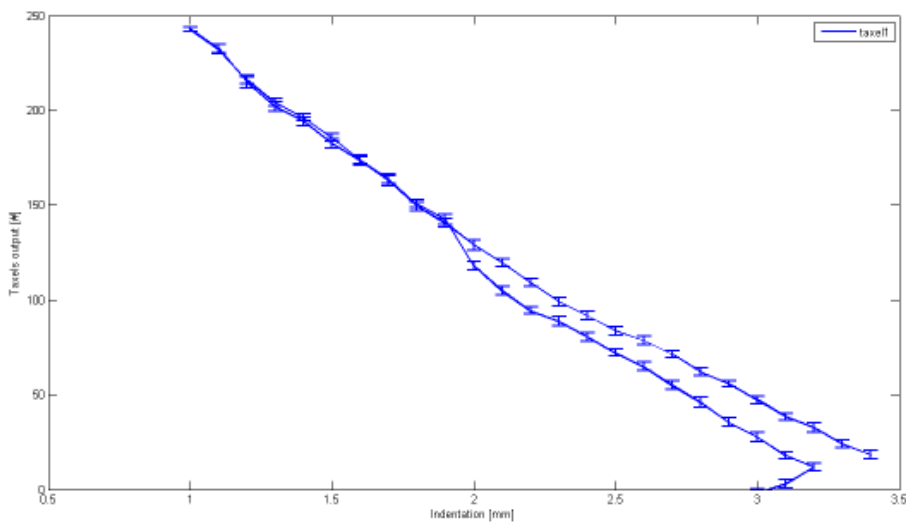


Figure 7.13: Taxels versus Deformation characteristic of one macro-area.

7. EXPERIMENTS

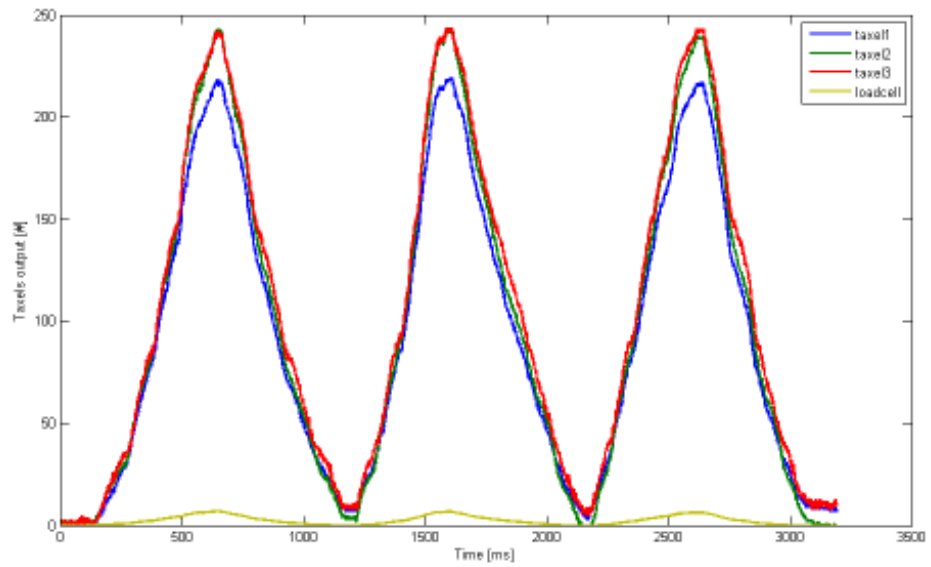


Figure 7.14: Load and Unload cycle reading three macro areas of the triangle

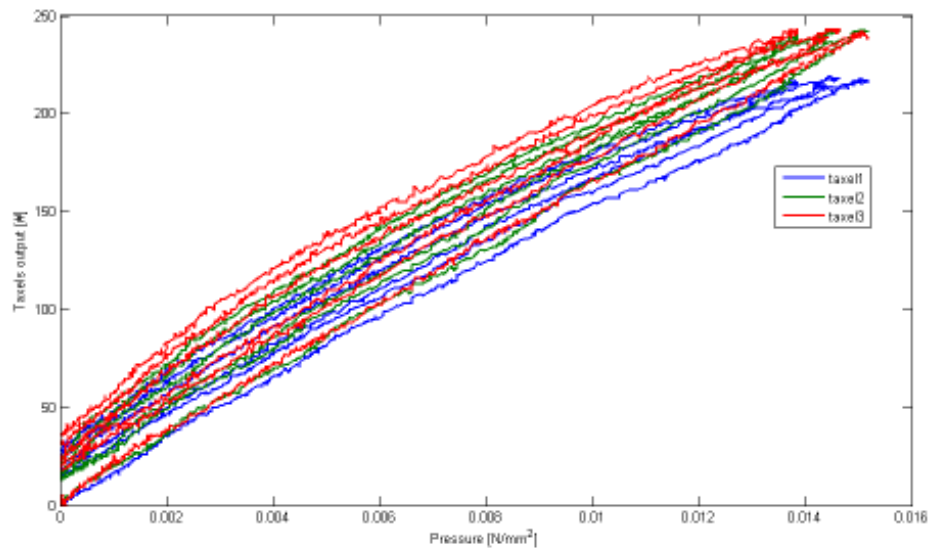


Figure 7.15: Taxels versus Loadcell characteristic reading three macro areas of the triangle

7.4 Third Experiment: Sensor Response with a uniform pressure distribution

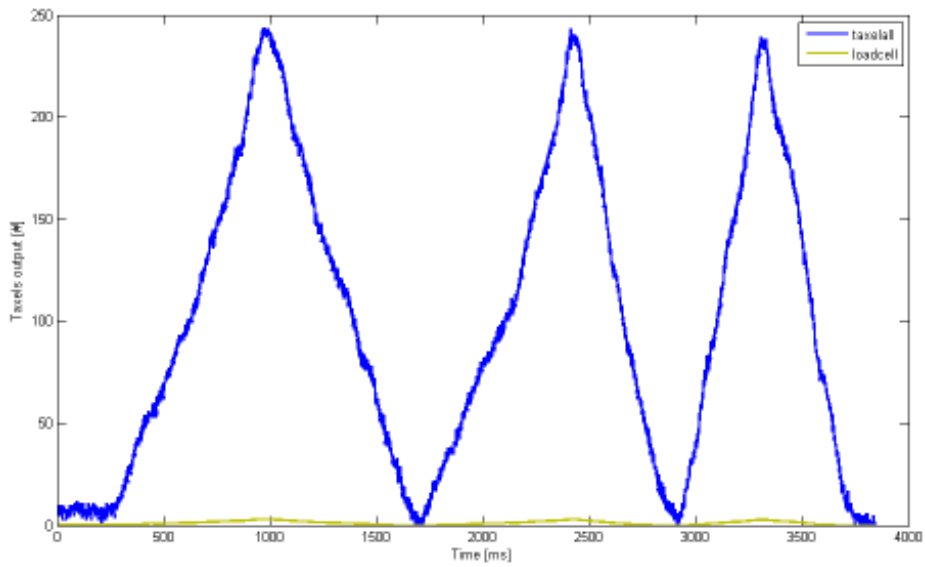


Figure 7.16: Load and Unload cycle reading one macro area of the triangle

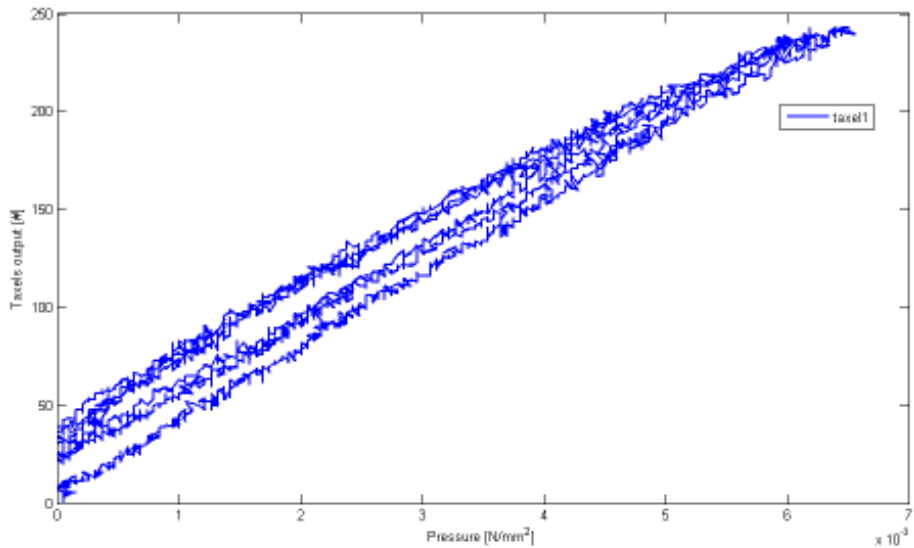


Figure 7.17: Taxels versus Loadcell characteristic reading one macro area of the triangle

7. EXPERIMENTS

7.18 . The experiments are executed for the three function mode of the sensor (twelve independent measurements, three and one macro-areas measurements).

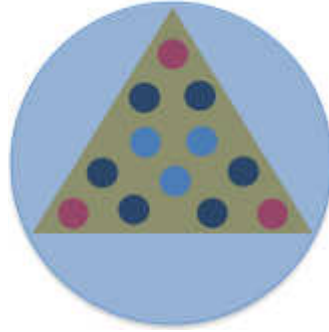


Figure 7.18: The circle represents the probe of the pressure, that in this case is bigger than the triangle. Therefore the pressure is uniform over the sensor.

7.5 Fourth Experiment: Static and Dynamic Response for a triangle covered by 1mm of neoprene

The experiment is analogous to the first experiment, but we have change the material as well as the thickness of the soft layer. The purpose of the test is to show how the response of the sensor changes, modifying the material. Therefore it is possible to tune the sensor response in order to obtain the desired range of measurements. Figures 7.26 and 7.27 shows the behavior of the sensor for the dynamic experiment (see section 7.3.1.2) and figure 7.28 graph the curve Taxels versus Deformation during in a static experiment (see section 7.3.1.1).

7.5 Fourth Experiment: Static and Dynamic Response for a triangle covered by 1mm of neoprene

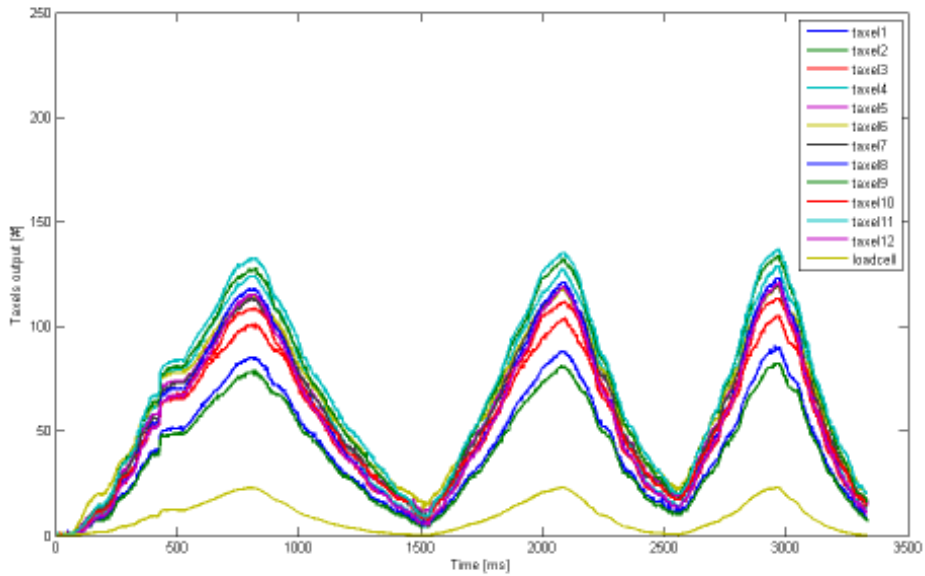


Figure 7.19: Load and Unload cycles for a uniform pressure over the triangle module

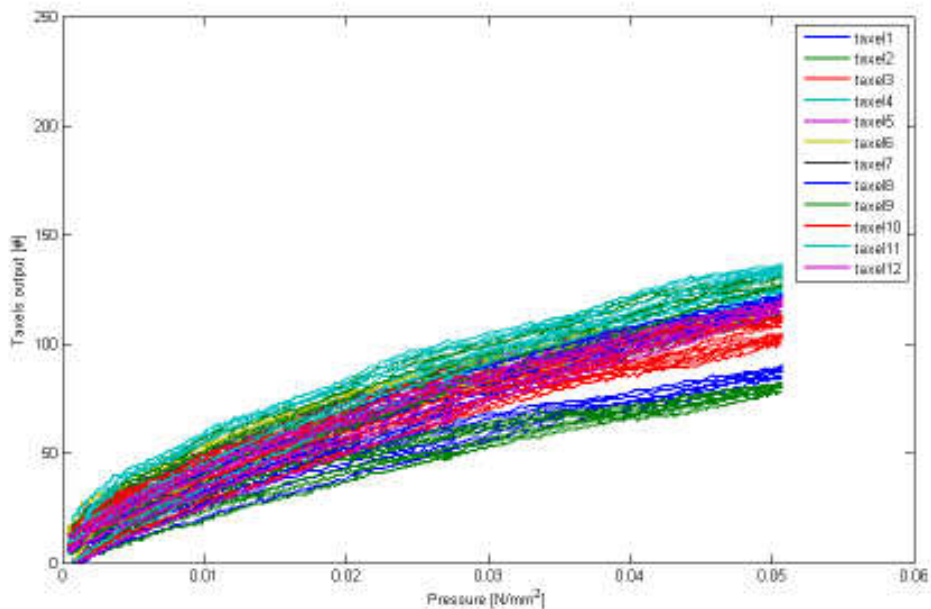


Figure 7.20: Taxels versus Loadcell characteristic for a uniform pressure over the triangle module

7. EXPERIMENTS

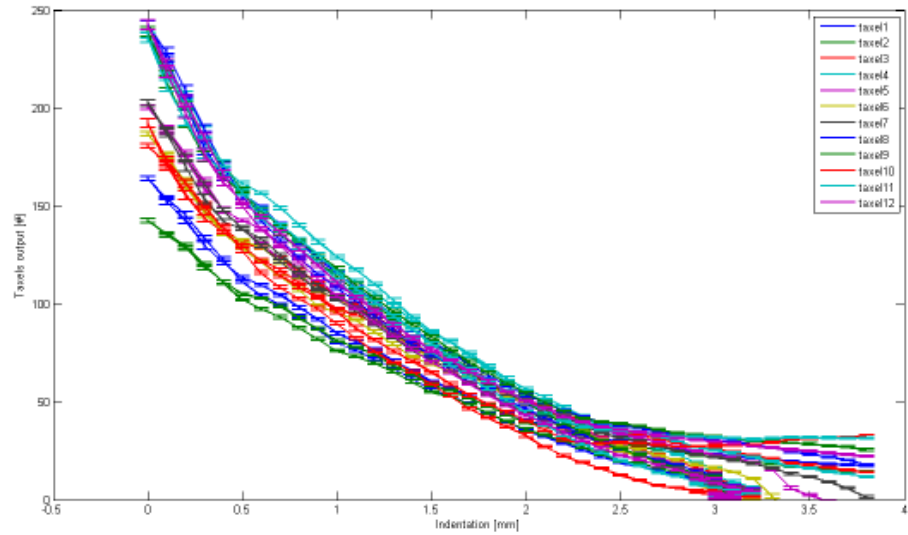


Figure 7.21: Taxels versus Deformation characteristic for a uniform pressure over the triangle module

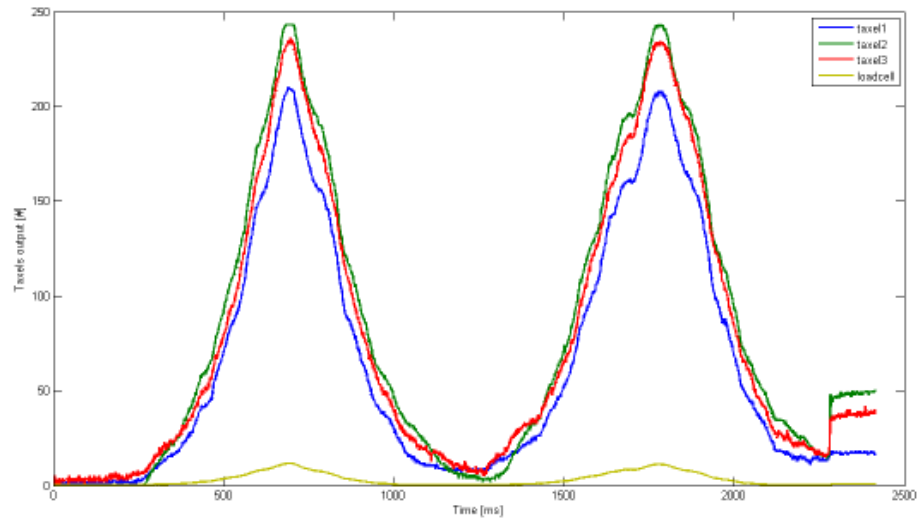


Figure 7.22: Load and Unload cycles reading three macro-areas for a uniform pressure over the triangle module

7.5 Fourth Experiment: Static and Dynamic Response for a triangle covered by 1mm of neoprene

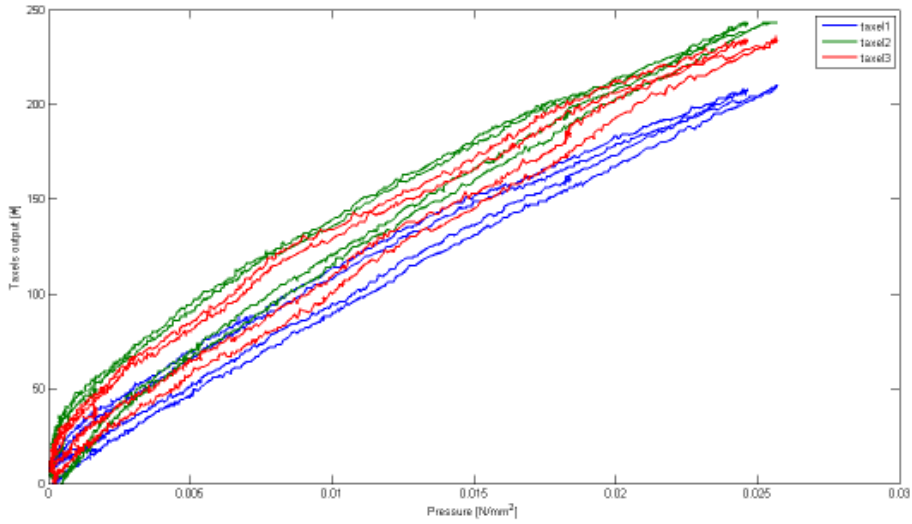


Figure 7.23: Taxels versus Loadcell characteristic reading three macro-areas for a uniform pressure over the triangle module

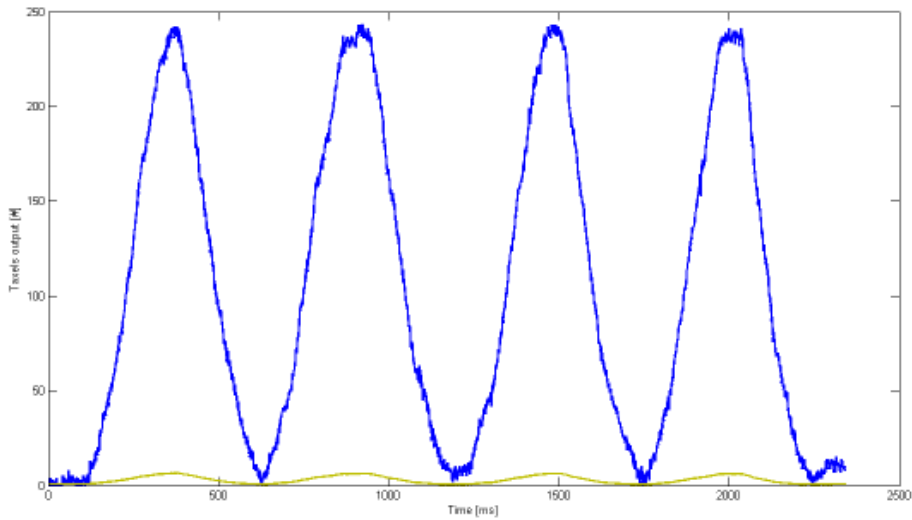


Figure 7.24: Load and Unload cycles reading one macro-area for a uniform pressure over the triangle module

7. EXPERIMENTS

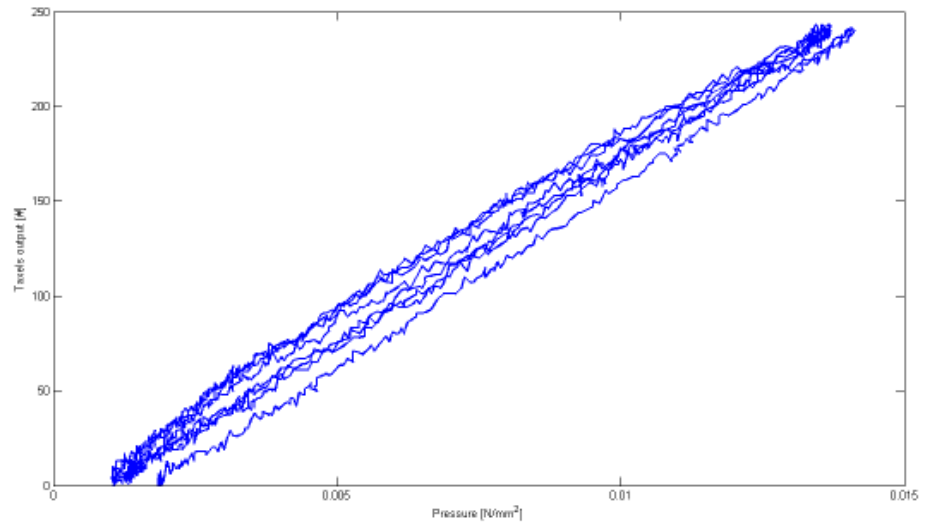


Figure 7.25: Taxels versus Loadcell characteristic reading one macro-area for a uniform pressure over the triangle module

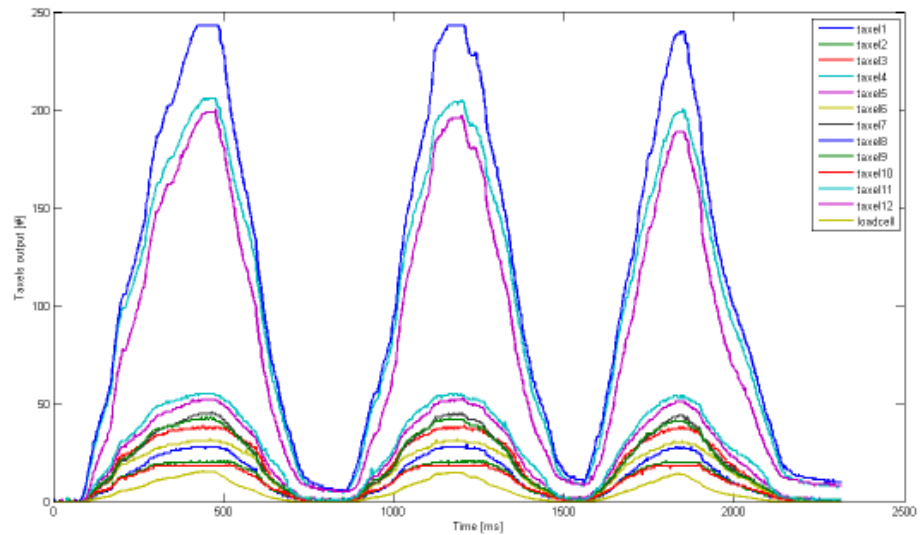


Figure 7.26: Load and Unload cycles for a 12mm probe positioned in the center of the triangle module

7.5 Fourth Experiment: Static and Dynamic Response for a triangle covered by 1mm of neoprene

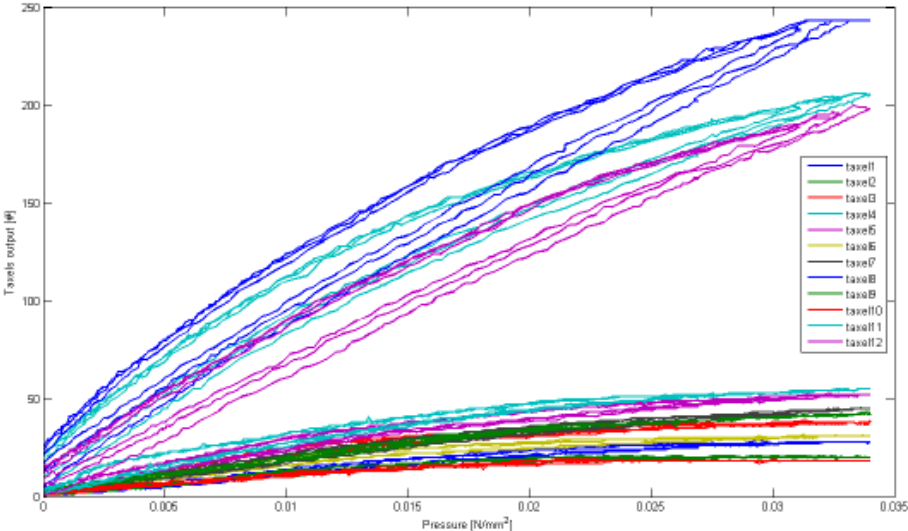


Figure 7.27: Taxels versus Loadcell curve for a 12mm probe positioned in the center of the triangle module

7. EXPERIMENTS

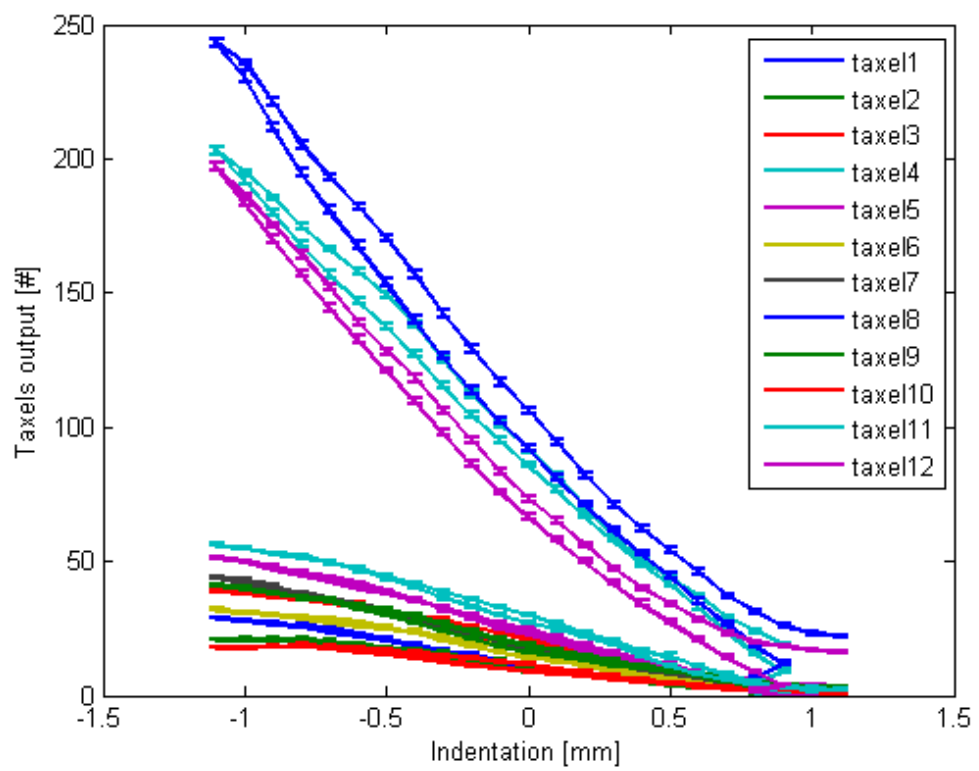


Figure 7.28: Taxels versus Deformation curve for a 12mm probe positioned in the center of the triangle module

Chapter 8

Discussion

The thesis has presented a possible solution for implementing a large area tactile sensor over the whole body of a robot. A system level approach has been used in order to design not only a prototype, but for installing it on a humanoid robot. In section 3.1 the guidelines we have used are summarized, here we discuss the how and if we have successfully complied with the specifications:

- **Conformability:** The skin can approximate curved surfaces. However the minimum radius of curvature with the current version is approximately 30-40 mm. Better results can be achieved by designing triangles with different size and shapes. From a preliminary study, triangles of 20 mm side can be done.
- **Compliance:** The outer layer of the sensor is silicone rubber, urethane foam or neoprene. Therefore it is compliant.
- **Dynamic range and sensitivity:** The dynamic range and the sensitivity can be changed by changing both the thickness and the stiffness of the soft layer.
- **Installation space:** each module has its own embedded electronics and is glued directly to the robot cover. Microcontroller boards are very compact and can be installed inside of the robot outer shell.

8. DISCUSSION

- Area coverage: It is possible to cover the whole robot with this solution. However for the fingers, we are designing an ad-hoc solution (Schmitz A. and G. (2008)), because of the very limited space.
- Weight: Silicone rubber foam, flex PCB are lightweight. The foam weights approximately 1 Kg for $1m^2$ of skin (the density of the foam is $240Kg/m^3$ and we consider a 4mm thick skin).
- Power consumption: The power consumed by the individual tactile elements is very low (3mW every 12 sensors).
- Size: The dimension of the single element is 4 mm in diameter.
- Toughness: The more fragile part, the flexible PCB is protected by silicone rubber. Therefore the robustness is guaranteed.
- Manufacturability: Until now, only small patches have been developed. An industrial procedure should be studied in order to produce large area sensors. However it is plausible that the result can be achieved in the near future.

8.1 Problems and Future Works

In the previous chapters we have seen the benefit of the proposed design. Now we want to talk about problems that we still have and future works. Triangle modules in the current version have the same size and shape. What we would do is to find the way to separate the geometry of the triangle from the electronics in a stack structure, in order to simplify the electronic design and to be able to build triangular module with any shape and size. For example, we could create an electronics core (with all the components on a very compact PCB) and then glue the layer with the pads on it, that can have different shapes. Another problem we have in the current implementation, regards the noise. We have seen that increasing the number of triangular modules, the level of noise increases. We are going to investigate the problem, but we think that with a more accurate PCB layout we can reduce the noise. Furthermore, despite the strategy that

8.1 Problems and Future Works

can be used to reduce the amount of data, the CANbus does not have enough bandwidth for a skin distributed on a whole robot's body. We are considering the use of a different solution, like for example a real-time Ethernet (e.g. EtherCat) or FlexRay. Future work, exploiting the robot skin technology will enable the study of tactile based control strategies for crawling and interact with humans.

8. DISCUSSION

Chapter 9

Publications

9.1 Journal publications

- 1 G. Cannata and M.Maggiali, "Models for the Design of Bio-Inspired Robot Eyes" IEEE TRANSACTION ON ROBOTICS - SPECIAL ISSUE ON BIO-ROBOTICS., , pag. 27-44, VOL. 24, NO. 1, February 2008.

Abstract: Active vision has the goal of improving visual perception; therefore the investigation of ocular motion strategies must play an important role in the design of humanoid robot eyes. Listings Law is a basic principle which characterizes various ocular movements in humans, including saccades and smooth pursuit, and its neural or mechanical origin has been debated for long time. Recent anatomical advances suggest that motions compatible with Listings Law could be mainly caused by the mechanical structure of the eye-plant. In this paper we present a bio-inspired model of the eye-plant, and we formally prove that, according to the model, the implementation of Listings Law can be actually explained on the base of the geometry of the eye and of its actuation system. The proposed model is characterized by a limited number of geometric parameters which can be easily used to set the guidelines for the design of humanoid, and possibly tendon driven, robot eyes. Simulative and experimental tests, performed on a robot prototype, are eventually presented to perform a quantitative evaluation of the performance of the model, also in comparison with physiological

9. PUBLICATIONS

data measured in humans and primates and reported in the literature.

9.2 Conference papers

- 1 G. Cannata, M. Maggiali "An Embedded Tactile and Force Sensor for Robotic Manipulation and Grasping" IEEE-RAS International Conference on Humanoid Robots Humanoids2005, December 5-7, 2005 Tsukuba.
- 2 G. Cannata, D. Biamino, M. Maggiali, A. Piazza: MAC-EYE: a Tendon Driven Fully Embedded Robot Eye" International Conference on Humanoid Robots Humanoids2005, December 5-7, 2005 Tsukuba.
- 3 G. Cannata, M. Maggiali: "Processing of Tactile/Force Measurements for a Fully Embedded Sensor" IEEE International Conference on Multisensor Fusion and Integration for Intelligent Systems, 3-6 September 2006.
- 4 G. Cannata, M. D'Andrea, M. Maggiali, F. Monti: ""Implementation of Listings Law for a Robot Eye" 8th International IFAC Symposium on Robot Control, September 6-8 2006 Bologna.
- 5 G. Cannata, M. Maggiali: "Implementation of Listings Law for a Tendon Driven Robot Eye" IROS 2006 Beijing, China 11-14 October 2006.
- 6 G. Cannata, M. D'Andrea, M. Maggiali, "Design of a Humanoid Robot Eye: Models and Experiments" International Conference on Humanoid Robots, Genova, 4-6 December 2006.
- 7 G. Cannata, M. Maggiali: "Processing of an Embedded Tactile Matrix Sensor", ROBIO 2006 Kunming, China 14-19 December 2006.
- 8 G.Cannata, M.Maggiali "Models for the Design of a Tendon Driven Robot Eye" International Conference on Robotics and Automation, ICRA 2007, 10-14 April 2007, Roma, Italy.
- 9 M.Maggiali, G. Cannata, P. Maiolino, G. Metta, M. Randazzo, G. Sandini, "Embedded Distributed Capacitive Tactile Sensor", Mechatronics 2008, June 23 25, University of Limerick, Ireland.

- 10 G. Cannata, M. Maggiali, G. Metta, G. Sandini "An Embedded Artificial Skin for Humanoid Robots" International Conference on Multi-sensor Fusion and Integration, 20-22 August 2008, Seoul, Korea.
- 11 Schmitz A., Maggiali M., Randazzo M., Natale L. and Metta G., "A Prototype Fingertip with High Spatial Resolution Pressure Sensing for the Robot iCub", IEEE International Conference Humanoids 2008, accepted for publication.

9.3 Book Chapters

- 1 G. Cannata and M. Maggiali, "Design of a Humanoid Robot Eye" Humanoid Robots New Developments, ISBN 978-3-902613-00-4, June 2007.
- 2 G. Cannata and M. Maggiali, "Design of a Tactile Sensor for Robot Hands", Sensors, Focus on Tactile, Force and Stress Sensors, in press.

9. PUBLICATIONS

Chapter 10

Patents

Maggiali M., Cannata G., Metta G., Sandini G. "Organization and placement of tactile elements for a haptic sensory system"

10. PATENTS

Appendix A

CANbus communication protocol

A.1 Introduction

This section contains a description of the CANBUS communication protocol. The CANbus is used from the Tactile Sensor Module (TMS) and the PC. The structure of the messages coming from the MCU to the PC is reported in table A.1.

where:

Message Class the class of the messages. 011 is the class for the TMSs messages

Source The identifier of the TSM (from 0 to 15).

Patch Relative Number The number of the triangle attached to the TMS (from 0 to 15).

Options In this field there are:

Bit[7] Message number (there are two messages for sending all the data coming from each triangle)

Bit[6] Resolution of measurements: 8 or 10 bits (respectively 0 and 1)

Bit[5] Not used

Bit[4] Not used

A. CANBUS COMMUNICATION PROTOCOL

Table A.1: Canbus Message frame

| CANbus Message | | | | |
|----------------|--------|-----------------------|---------|-----------|
| 3 bits | 4 bits | 4 bits | data[0] | data[1-7] |
| Message Class | Source | Patch Relative Number | Options | PayLoad |

Table A.2: Command Frame

| CANbus Message | | | | |
|----------------|--------|-------------|----------------|-----------|
| 3 bits | 4 bits | 4 bits | data[0] | data[1-7] |
| Message Class | Source | Destination | C Message Type | PayLoad |

Bit[0-3] These fields are filled with Pressure Measurements

PayLoad These fields are filled with Pressure Measurements.

A.1.1 Protocol Command Messages

There is a list of polling messages from the PC to the TSM that are used to set up the microcontroller and to change the parameters regarding the triangle modules. The list is presented below together with a brief description of each message. The structure of the data frame is reported in table A.2.

where:

Message Class the class of the messages. 001 is the class for the polling messages

Source The identifier (ID) of the source (the ID of the PC is 0).

Destination The ID of destination board (from 0 to 15).

C It is a bit that is used in the motor control board for specifying the channel number. Here it is set to 0.

Message Type The type of message.

Payload These fields are filled with different values depending on the message type.

For any Message Type the payload and the length of the packet changes. Here are reported the main type of messages used for setting up the TSM:

CAN_SET_ADDITIONAL_INFO It is possible to assign a description of 48 characters to the TSM. 8 messages can be used to send the string.

Message Type 13

Payload data[1] message number, data[2-7] chars.

CAN_GET_ADDITIONAL_INFO It is possible to read the description of 48 characters to the TSM.

Message Type 12

Payload data[1] message number, data[2-7] chars.

CAN_TACT_SETUP **Message Type** 12

Payload data[1 bits 0-3] Measures resolution: 0 for 16 bits, 1 for 8 bits and 2 for 10 bits.

data[1 bits 4-7] Triangles Configuration: 0 for 12 measures(SINGLE), 1 for 3 measures (MULTI)

data[2] CDC converter resolution: 1 for max resolution, 2 for medium and 3 for low.

data[3] Sampling rate. There are 3 different sampling rate: 30 Hz, 50 Hz and selectable by data[6] and data[7].

data[4-5] CDC capacitance offset. This is the offset of the CDC. For SINGLE configuration 0x0700 is a good number. For MULTI, 0x0020 is ok.

data[6-7] Timer value. This value is multiplied by 3.2e-6 (64*20e6) to obtain the value in seconds

A. CANBUS COMMUNICATION PROTOCOL

Appendix B

Triangular Module Schematic and Layout

B.1 Introduction

In this section the schematic and the layout of the MCU board is reported.

B. TRIANGULAR MODULE SCHEMATIC AND LAYOUT

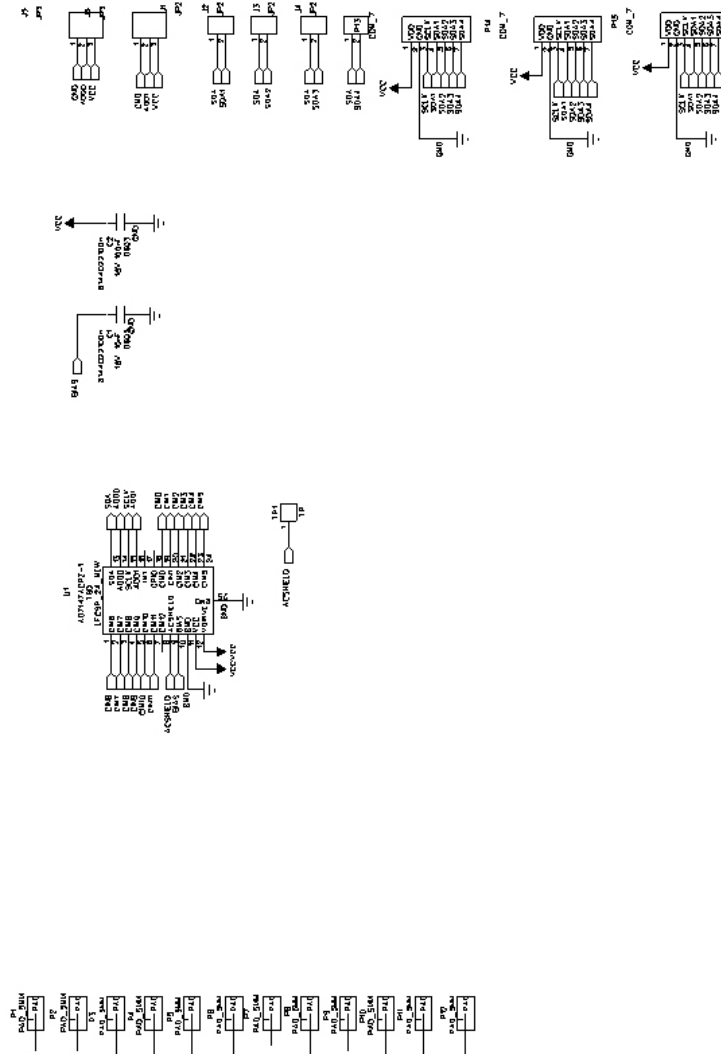


Figure B.1: Schematic of the triangle module

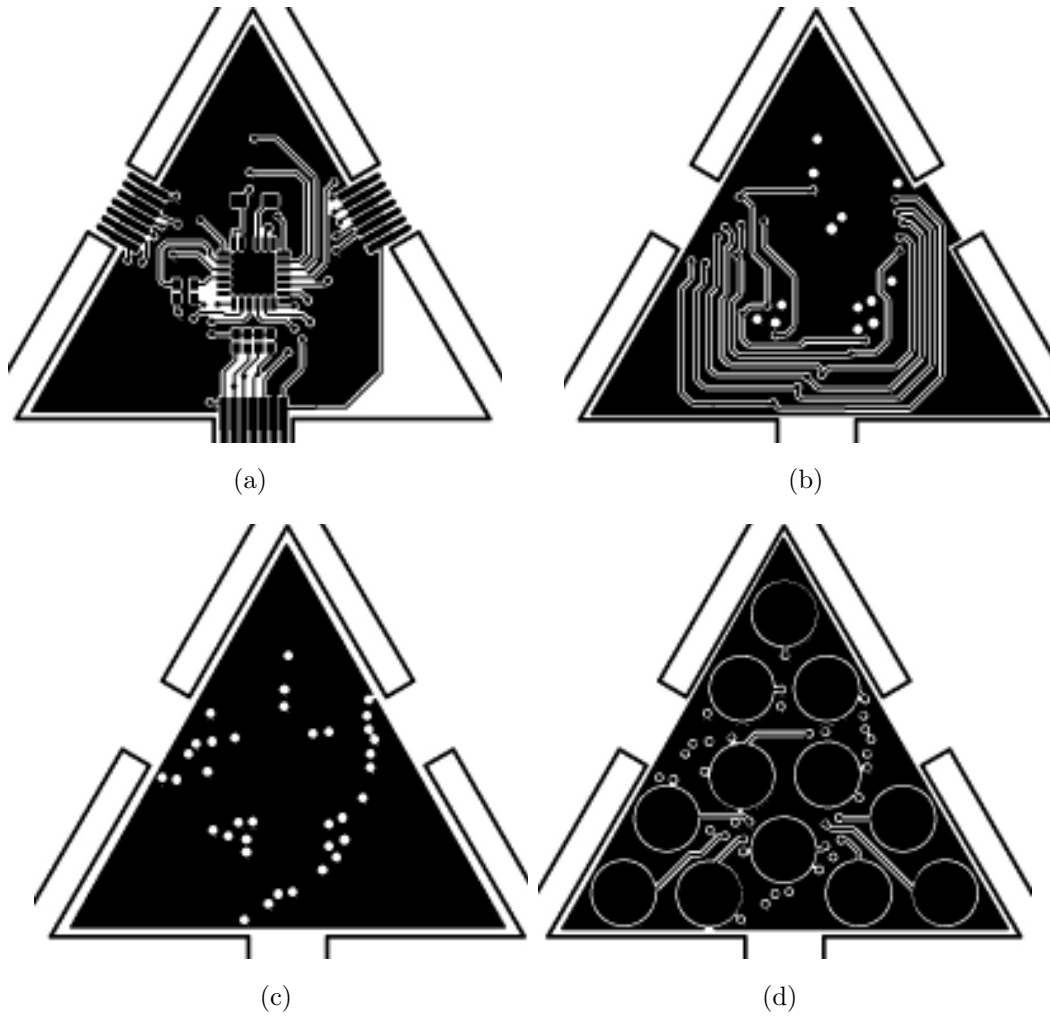


Figure B.2: Layout of the triangle module, top (A), inner layer 1(B) and 2 (C) and bottom (D)

B. TRIANGULAR MODULE SCHEMATIC AND LAYOUT

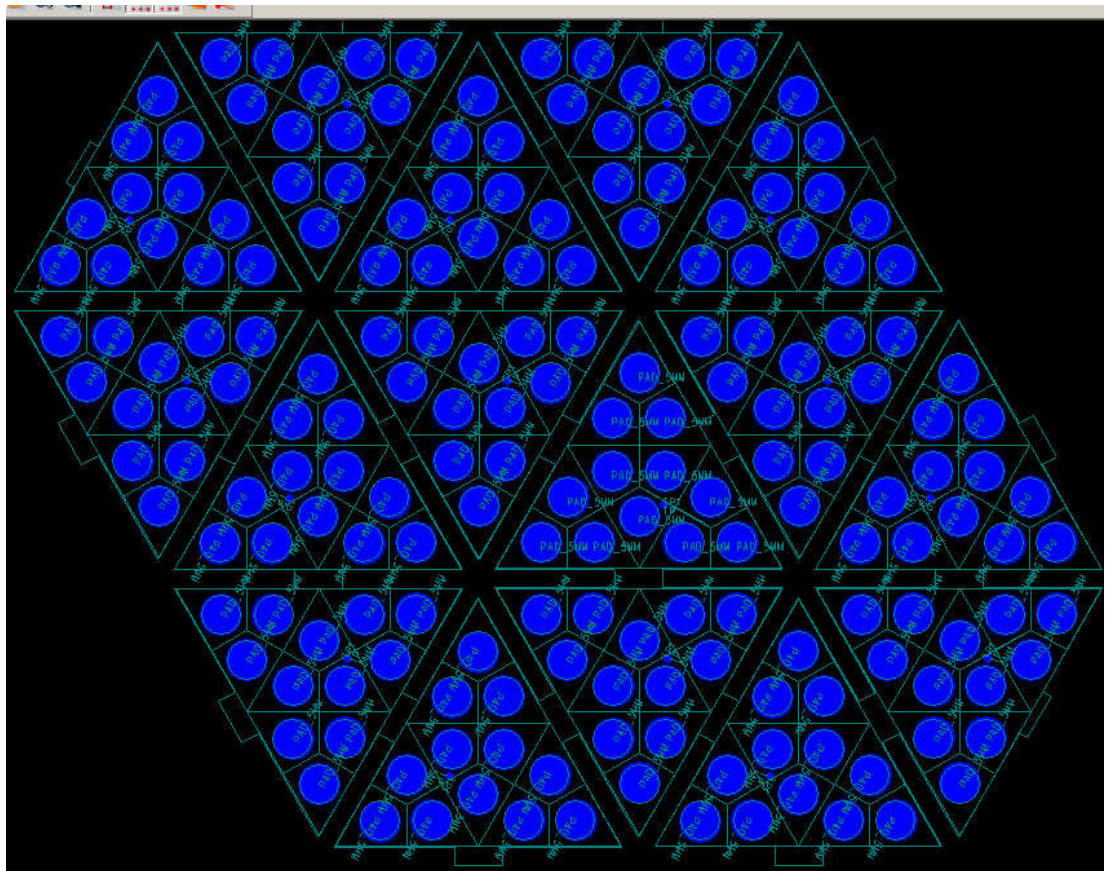


Figure B.3: Layout of the triangles sheet

Appendix C

MCU Module Schematic and Layout

C.1 Introduction

In this section the schematic and the layout of the MCU board is reported.

C. MCU MODULE SCHEMATIC AND LAYOUT

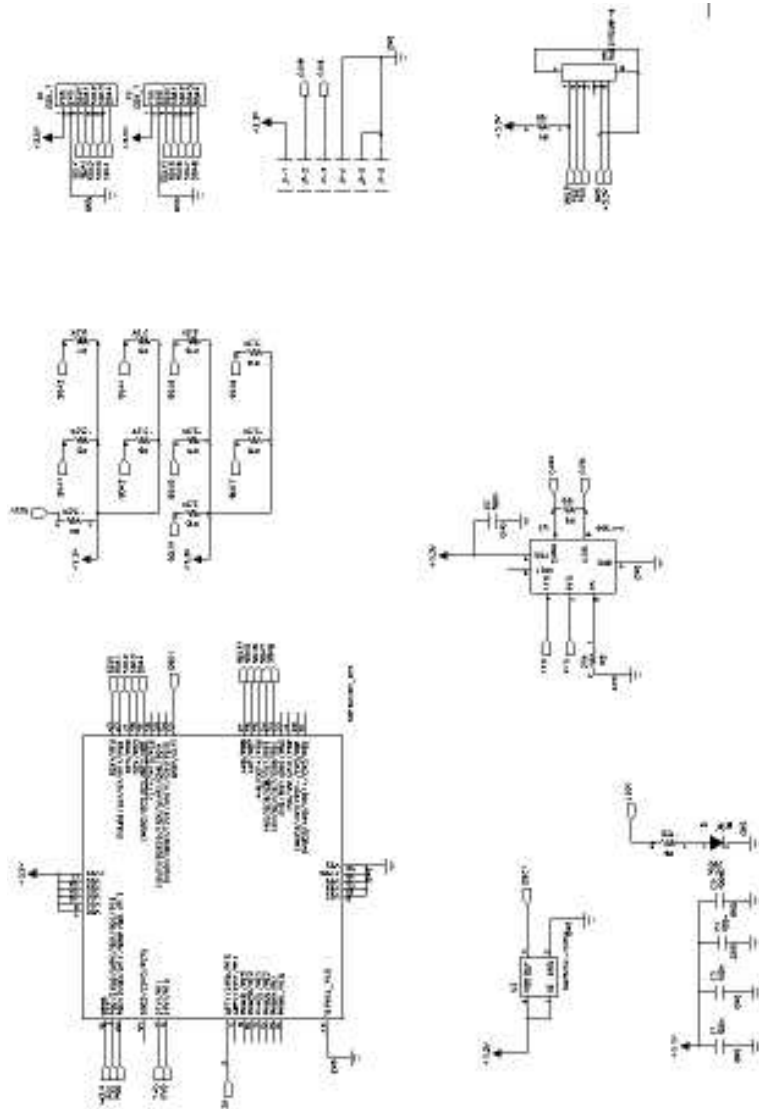
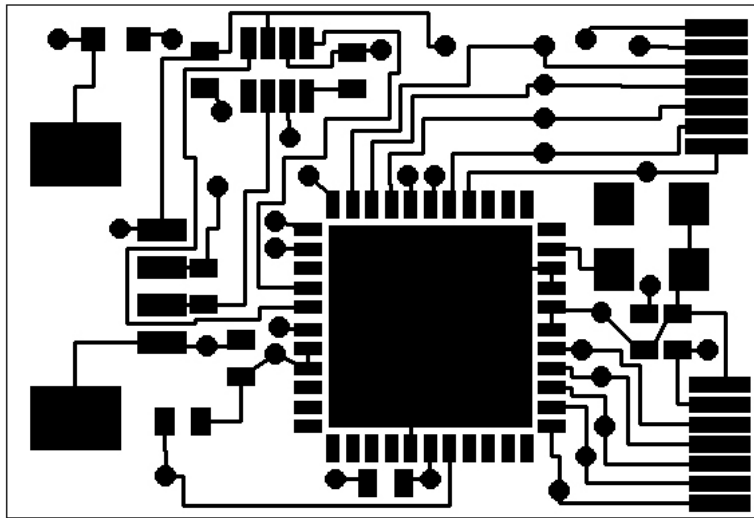
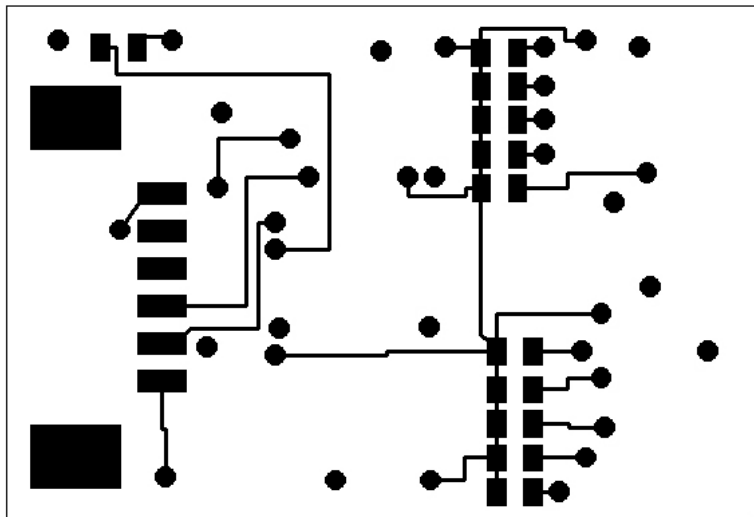


Figure C.1: Schematic of the MCU board



(a)



(b)

Figure C.2: Layout of the MCU board, top (A) and bottom (B)

C. MCU MODULE SCHEMATIC AND LAYOUT

References

- A. Billard and R. Siegwart. Robot learning from demonstration. *Journal of Robotics and Autonomous Systems*, 47:65–67, 2004. 10
- J.J. Cabibihan B.B. Edin, L. Beccai and M.C. Carrozza. A bio-inspired approach for the design and characterization of a tactile sensory system for a cybernetic prosthetic hand. In *Proceedings of the 2006 IEEE International Conference on Robotics and Automation*, 2006. 3, 7
- J.K. Salisbury Bicchi. A and D.L. Brock. Contact sensing from force measurements. *International Journal of Robotics Research*, 12(3):249–262, June 1993. 4
- Hirzinger G. Butterfass J., Grebenstein M. Dlr-hand ii: next generation of a dextrous robot hand. In *Proc. IEEE Int. Conf. on Robotics and Automation*, 2001. v, 4, 5, 6
- Um D. and V. Lumelsky. Fault tolerance via analytic redundancy for a modularized sensitive skin. In *Proceedings of the IEEVRSJ International Conference on Intelligent Robots and Systems*, 1999. 12
- Analog. Device. Ad7147 technical datasheet. *www.analog.com*, 2008. 33, 35, 43
- Selby J. C. Engel J., Chen J. and A. M. Shannon. Development of polyimide-based flexible tactile sensing skin. In *Mat. Res. Soc. Symp. Proceedings*, volume 736, 2003. 4
- Cannata G. and Maggiali M. An embedded tactile and force sensor for robotic manipulation and grasping. In *Proceeding of IEEE-RAS International Conference on Humanoid Robots*, 2005. 3

REFERENCES

- Cannata G. and Maggiali M. Processing of tactile/force measurements for a fully embedded sensor. In *International Conference on Multisensor Fusion and Integration for Intelligent Systems*, 2006. 22
- T. Komatsu H. Kawasaki, T. Komatsu and K. Uchiyama. Dexterous anthropomorphic robot hand with distributed tactile sensor: Gifu hand ii. *Transaction on Mechatronics*, 7(3):296–303, 2002. v, 3, 5, 6
- P. Meusel H. Liu and G. A. Hirzinger. A tactile sensing system for the three-finger robot hand. In *International Symposium on DLR Measurement and Control in Robotics*, pages 91–96, 1995. 3
- T. Nishino I. Mizuuchi, T. Yoshikai and M. Inaba. Development of musculoskeletal humanoid kotaro. In *Proceedings of the 2006 IEEE International Conference on Robotics and Automation*, 2006. v, 15, 16
- M. H. Lee and H. R. Nicholls. Tactile sensing for mechatronics a state of the art survey. *Mechatronics*, 9:1–31, 1999. 3, 18
- Shur M.S. Lumelsky V.J. and Wagner S. Sensitive skin. *IEEE Sensors Journal*, 1(1):41–51, June 2001. 10
- Krishna G. M. and Rajanna K. Tactile sensor based on piezoelectric resonance. *Sensors*, 2:1643– 1647, 2002. 4
- Shimojo M. A tactile sensor sheet using pressure conductive rubber with electrical wires stitched method. *IEEE Sensor Journal*, 4(5), 2004. 4
- Microchip. dspic30f4011 technical datasheet. *www.microchip.com*, 2008. 46
- Hirano S. Mukai T., Onishi M. and Luo Z. Development of the tactile sensor system of a human-interactive robot ri-man”. *IEEE Transactions on Robotics*, 24(2):505–512, April 2008. 12, 13
- Randazzo M. Natale L. Schmitz A., Maggiali M. and Metta G. A prototype fingertip with high spatial resolution pressure sensing for the robot icub. In *IEEE International Conference, Humanoids 2008*, 2008. 80

REFERENCES

- J. Schroder T. Asfour, K. Regenstein and Dillmann R. Armar-iii: A humanoid platform for perception-action integration. In *International Workshop on Human-Centered Robotic Systems*, 2006. v, 3, 12, 13, 21
- R. O. Ambrose T. B. Martin and M. J. Butzer. Tactile gloves for autonomous grasping with the nasa/darpa robonaut. In *IEEE International Conference on Robotics and Automation*, 2004. v, 3, 7, 9
- H. Ishiguro T. Minato, Y. Yoshikawa and Asada M. Cb2: A child robot with biomimetic body for cognitive developmental robotics. In *IEEE-RAS 7th International Conference on Humanoid Robots*, 2007. v, 12, 15, 16, 21
- J. Takai T. Mouri, H. Kawasaki and S. Ito. Anthropomorphic robot hand: Gifu hand iii. In *ICCAS*, 2002. v, 5, 6
- Miyashita T. Tajika T. and Ishiguro H. Automatic categorization of haptic interactions-what are the typical haptic interactions between a human and a robot? In *Proceeding of IEEE-RAS International Conference on Humanoid Robots*, 2006. v, 3, 12, 14
- Y. Kuniyoshi Y. Ohmura. Humanoid robot which can lift a 30kg box by whole body contact and tactile feedback. In *Proceedings of the 2007 IEEE/RSJ International Conference on Intelligent Robots and Systems*, 2007. 10, 11
- Y. Kuniyoshi Y. Ohmura and A. Nagakubo. Conformable and scalable tactile sensor skin for curved surfaces. In *Proceedings of the 2006 IEEE International Conference on Robotics and Automation*, 2006. vi, 10, 11, 17, 21, 22
- Koshida N. Yamada K., Goto K. and H. Shinoda. A sensor skin using wire-free tactile sensing elements based on optical connection. *Sice*, 1:131–134, 2002. 4

Declaration

I herewith declare that I have produced this paper without the prohibited assistance of third parties and without making use of aids other than those specified; notions taken over directly or indirectly from other sources have been identified as such. This paper has not previously been presented in identical or similar form to any other Italian or foreign examination board.

Genova,